Modeling, Analysis and Testing of an Electrostatically Actuated Waveguide based Optical MEMS device for Variable Optical Attenuation

SRINIVASA RAGHAVENDRA PENDYALA

A Thesis

in

The Department

of

Mechanical and Industrial Engineering

Presented in partial fulfillment of the requirements for the
Degree of Master of Applied Science (Mechanical Engineering) at
Concordia University
Montreal, Quebec, Canada

August 2007

© Srinivasa Raghavendra Pendyala 2007

Library and Archives Canada

Published Heritage Branch

395 Wellington Street
Ottawa ON K1A 0N4
Canada

Bibliothèque et Archives Canada

Direction du Patrimoine de l'édition

395, rue Wellington
Ottawa ON K1A 0N4
Canada

Your file Votre référence
ISBN: 978-0-494-34716-4
Our file Notre référence
ISBN: 978-0-494-34716-4

NOTICE:
The author has granted a non-exclusive license allowing Library and Archives Canada to reproduce, publish, archive, preserve, conserve, communicate to the public by telecommunication or on the Internet, loan, distribute and sell theses worldwide, for commercial or non-commercial purposes, in microform, paper, electronic and/or any other formats.

AVIS:
L'auteur a accordé une licence non exclusive permettant à la Bibliothèque et Archives Canada de reproduire, publier, archiver, sauvegarder, conserver, transmettre au public par télécommunication ou par l'Internet, prêter, distribuer et vendre des thèses partout dans le monde, à des fins commerciales ou autres, sur support microforme, papier, électronique et/ou autres formats.

The author retains copyright ownership and moral rights in this thesis. Neither the thesis nor substantial extracts from it may be printed or otherwise reproduced without the author's permission.

L'auteur conserve la propriété du droit d'auteur et des droits moraux qui protège cette thèse. Ni la thèse ni des extraits substantiels de celle-ci ne doivent être imprimés ou autrement reproduits sans son autorisation.

In compliance with the Canadian Privacy Act some supporting forms may have been removed from this thesis.

Conformément à la loi canadienne sur la protection de la vie privée, quelques formulaires secondaires ont été enlevés de cette thèse.

While these forms may be included in the document page count, their removal does not represent any loss of content from the thesis.

Bien que ces formulaires aient inclus dans la pagination, il n'y aura aucun contenu manquant.

ABSTRACT

Modeling, Analysis and Testing of an Electrostatically Actuated Waveguide based Optical MEMS device for Variable optical attenuation

Srinivasa Raghavendra Pendyala

Electrostatic actuation is a promising solution for Micro Electro Mechanical Systems because of its good scaling properties in small dimensions, high-energy densities and relative ease of fabrication. Its low response time and compatibility with IC technologies make it even more suitable for the optical applications, such as, optical switching and Variable Optical Attenuators (VOAs) in telecommunications. Variable Optical Attenuators are very important components in fiber optic communication systems needed throughout the network to control optical power and prevent the saturation of receivers.

This thesis describes the design of a novel and simple electrostatically actuated variable optical attenuator that uses the electrostatic actuation of a cylindrical waveguide. The proposed device stands out from the existing conventional optical attenuators by directly moving the input waveguide for creating misalignment and thus eliminating the need for extra optical components required in free space. This model has capability for a high dynamic range of attenuation and has other advantages of low wavelength dependent loss and low back reflection. The optical MEMS device consists of a metal coated cylindrical waveguide positioned in a V-groove and overhanging at the end to act as a free standing cantilever.

This work presents modeling, analysis and testing of the proposed device. The system has been defined accurately using coupled electromechanical models that take into account the capacitance of the cylindrical electrode configuration. The static and dynamic analyses of the system have been performed using the Rayleigh Ritz energy method. The developed electromechanical model is generic and could be applied to any cylindrical electrostatic actuator. The generality of the method has been demonstrated in this work by performing static and dynamic analysis on a carbon nanotube actuator and nano resonator, respectively, using the above model. To verify the feasibility of the method for optical attenuation parametric study is presented and the resulting static deflections, pull-in voltages, natural frequencies and finally achieved attenuation have been presented.

Testing is a very vital component in the synthesis of a microsystem. Experimental testing is carried out in this work using non contact optical methods. Both static testing using optical microscope and dynamic testing using Laser Doppler Velocimetry have been performed on a prototype representing the proposed device. The experimental results of deflection were found to be in good agreement with the theoretical results from the model.

DEDICATED TO

MY PARENTS

ACKNOWLEDGEMENTS

The author is deeply privileged to work with Dr. Muthukumaran Packirisamy and likes to thank him for his valuable guidance, encouragement and the enlightening discussions had during the Thesis work. I also want to thank him for the timely help in pulling me out of the infinite loops, when I am stuck at the same point and redirecting me when taking the wrong exits while exploring the relatively new research area of the thesis. This work is a product of many interesting experiences, hard work and fun.

The author is also inspired by Dr.Bhat who always emphasizes the importance of strong foundation in the fundamentals before building complex systems. The author would also like to thank Dr. Ion Stiharu for the encouragement and concern shown in the work. Author would like to thank the Concordia University in entirety for transforming him from a student to professional with exposure to real world.

I would definitely thank Dr. Petre Tzenov for conferring many teaching assistantships which were very helpful in improving my expression and personality while serving as a financial support.

The author enjoys the company of his colleagues in the research lab and thanks all of them for the great time. I also want to thank my friend Lakshmi Narayana for all the advice and help given at the start of the program. I also want to acknowledge the

beautiful city of Montréal and the friends I met who made the life colorful and interesting during the time of my work.

Most importantly, Iam thankful to Satvik, Bujji and Baava for their unconditional support and letting me launch in Montréal. I am very thankful to my parents who always supported and encouraged me to success in every step of my life and this thesis is dedicated to them. Finally thank God for everything good in life.

TABLE OF CONTENTS

ABSTRACT iii

ACKNOWLEDGEMENTS vi

LIST OF FIGURES xi

LIST OF TABLES xiv

NOMENCLATURE xv

SYMBOLS xvii

CHAPTER 1 INTRODUCTION 1

1.1 INTRODUCTION TO MEMS 1

1.2 ACTUATION 3

1.2.1 THERMAL ACTUATION 4

1.2.2 PIEZOELECTRIC ACTUATION 4

1.2.3 ELECTROMAGNETIC ACTUATION 5

1.2.4 ELECTROSTATIC ACTUATION 5

1.3 TYPES OF ELECTROSTATIC ACTUATORS 5

1.4 ATTENUATION 7

1.5 TYPES OF ATTENUATION 9

1.5.1 NON-WAVEGUIDE ATTENUATION SCHEMES 10

1.5.2 WAVEGUIDE ATTENUATION 15

1.6 RATIONALE AND OBJECTIVE OF THE THESIS 18

1.7 ORGANIZATION AND LAYOUT OF THE THESIS 19

CHAPTER 2 STATIC MODELING AND ANALYSYS 21

2.1 INTRODUCTION TO MEMS MODELING 21

2.2 MODELING ELECTROSTATIC ACTUATION 22

2.2.1 NONLINEARITY 24

2.2.2 ELECTROMECHANICAL COUPLING 25

2.2.3 PULL-IN PHENOMENON 26

2.2.4 RESIDUAL CHARGES 27

2.3 ELECTROSTATIC MODELING OF THE SYSTEM 28

2.4 MECHANICAL MODEL OF THE SYSTEM 31

2.5 COUPLED ELECTROMECHANICAL MODEL AND SOLUTION 31

2.6 VALIDATION OF THE MODEL 36

2.7 SUMMARY 38

CHAPTER 3 DYNAMIC MODELING 39

3.1 INTRODUCTION 39

3.2 EXISTING METHODS OF DYNAMIC ANALYSIS 40

3.3 DYNAMIC MODELING METHOD USED IN THE THESIS 44

3.3.1 BOUNDARY CHARACTERISTIC ORTHOGONAL POLYNOMIALS 48

3.3.2 ELASTIC FOUNDATION 51

3.4 VALIDATION OF THE MODEL 54

3.5 SUMMARY 56

CHAPTER 4 DESIGN OF A VARIABLE OPTICAL ATTENUATOR 57

4.1 INTRODUCTION TO VOA DESIGN 57

4.2 PROPOSED VOA DESIGN 58

4.3 OPTICAL MODELING 60
4.4 DESIGN CRITERION 62
4.5 PARAMETRIC STUDY 63
4.6 DYNAMIC ANALYSIS 67
4.7 SUMMARY 69
CHAPTER 5 EXPERIMENTAL ELECTROMECHANICAL TESTING 70
5.1 INTRODUCTION 70
5.2 EXISTING TESTING TECHNIQUES 71
5.3 STATIC TESTING 74
5.3.1 TEST SET UP 74
5.3.2 TEST DEVICE PREPARATION 75
5.3.3 MEASUREMENT OF TIP DEFLECTION 78
5.4 RESULTS, OBSERVATIONS AND DISCUSSIONS 80
5.5 DYNAMIC TESTING 83
5.5.1 TEST SETUP 84
5.5.2 TESTING PROCEDURE 86
5.6 RESULTS AND DISCUSSIONS 88
5.7 SUMMARY 89
CHAPTER 6 CONCLUSIONS 90
6.1 CONCLUSIONS 90
6.2 CONTRIBUTIONS 92
6.3 RECOMMENDATIONS FOR FUTURE WORK 93

LIST OF FIGURES

Figure 1.1: A 4:1 pressure ratio, 4 mm rotor diameter radial in flow turbine stage. [2]..... 2

Figure 1.2: WDM network showing various components [8] 8

Figure 1.3: Scanning electron micrograph of a dual shutter attenuator driven by a comb drive [19].. 11

Figure 1.4: SEM image of a Retro VOA using two coaxial mirrors driven by comb drives [22]. 13

Figure 1.5: MARS type modulator based on Mach Zehnder interferometry showing both phases of attenuation [23]. 14

Figure 1.6: A fiber actuated optical switch by a comb drive [32]. 18

Figure 2.1: Block diagram showing the modeling tools often used in mechanical product design 22

Figure 2.2: Schematic of parallel plate actuation.. 23

Figure 2.3: Schematic showing the electric fields induced on a cylindrical electrostatic actuator.. 29

Figure 2.4: Schematic showing the deflected electrostatic actuator. 30

Figure 2.5: Linear mechanical force and nonlinear electrostatic forces evaluated for various voltages.. 34

Figure 2.6: Comparison of values of tip gap of the actuator obtained from the theoretical model with the literature [49].. 37

Figure 3.1: Typical transient response curve for an electrostatic actuator [54]................ 42

Figure 3.2: Schematic line diagram showing the mode shape of a vibrating cantilever... 45

Figure 3.3: Elastic foundation representation of the electrostatically actuated waveguide. 51

Figure 3.4: Typical force balance curve showing the point of linearization for small amplitude of vibrations 52

Figure 3.5: Variation of K_{ES} for an applied voltage of 10V and an electrode gap of 60 microns. 54

Figure 3.6: Mode shapes of carbon nano resonators A) at no voltage and noise, B) First mode, C) second mode [60] 55

Figure 4.1: Typical MEMS Design Methodology 58

Figure 4.2: Schematic of the electrostatically actuated cylindrical waveguide based variable optical attenuator 59

Figure 4.3: Exaggerated Schematic showing attenuating fiber due to lateral and angular misalignment 61

Figure 4.4: Tip deflection of waveguide for an electrode gap of 60 microns for various voltages 64

Figure 4.5: Tip deflection of waveguide for an electrode gap of 30 microns for various voltages 64

Figure 4.6: Coupling efficiency of waveguide for an electrode gap of 60 microns for various voltages. 65

Figure 4.7: Coupling efficiency of waveguide for an electrode gap of 30 microns for various voltages. 65

Figure 4.8: Insertion loss/attenuation for an electrode gap of 60 microns for various voltages 66

Figure 4.9: Insertion loss or attenuation for an electrode gap of 30 microns for various voltages 66

Figure 4.10: Natural frequency Vs voltage for various lengths of waveguides at an electrode gap of 60 microns 68

Figure 4.11: Natural frequency Vs voltage for various lengths of waveguides and electrode gap of 30 microns 68

Figure 5.1: Experimental test set up for static deflection measurement 75

Figure 5.2 : Schematic of the experimental static deflection test setup 77

Figure 5.3: Close up of the MEMS VOA device under test. 78

Figure 5.4: Variation of tip deflection against applied voltage for the Design S 81

Figure 5.5: Variation of tip deflection against applied voltage for the Design L 81

Figure 5.6: Flames appearing due to the Electric discharge when the top electrode approaches bottom electrode. 83

Figure 5.7 : Testing setup using Laser Doppler Velocimetry. 85

Figure 5.8: Close up view of the device mounted on an xyz positioner for aligning with the Laser 85

Figure 5.9: reflective tape used to increase the intensity of the reflected laser beam signal 87

Figure 5.10: Frequency response of Device S with electrostatic excitation 88

LIST OF TABLES

Table 2.1: Properties of the silica cylindrical waveguides used for static analysis. 35

Table 2.2: Properties and dimensions of the nano actuator used for theoretical validation 37

Table 3.1: Comparison of the model results of natural frequencies with values from literature [60] 55

Table 3.2: List of parameters used in the validation of the model. 55

Table 5.1: Property values and dimensions of waveguides used in experiments. 77

Table 5.2: Experimental measurements on the ocular of the microscope for a 15 mm fiber actuator Devices. 79

Table 5.3: Dimensions and mechanical properties of the reflective tape 87

Table 5.4: Comparison of natural frequencies for Device S 88

NOMENCLATURE

AC	Alternating Current
AFM	Atomic Force Microscope
AM	Amplitude Modulation
CMOS	Complementary Metal Oxide Semiconductor
dB	Decibel
DC	Direct Current
DWDMS	Dense Wavelength Division Multiplexing Systems
DWNT	Double Walled Nano Tube
FEM	Finite Element Method
FM	Frequency Modulation
LC	Liquid Crystal
LDV	Laser Doppler Velocimetry
LED	Light Emitting Diode
MARS	Mechanically Active Anti-reflection Switch
MEMS	Micro -Electro-Mechanical Systems
MOEMS	Micro-Opto-Electro-Mechanical Systems
MST	Micro Systems Technology
PDL	Polarisation Dependant Loss
PDMS	Polydimethylsiloxane
PLZT	Lead-Lanthanum-Zirconate-Titanate
PM	Phase Modulation

PSI	Phase Shifting Interferometry
PVDF	PolyvinylideneDiflouride
PZT	Piezoelectric Lead zirconium Titanate
RF	Radio Frequency
RL	Return loss
RPM	Revolutions per minute
SEM	Scanning Electron Microscopy
Si	Silicon
SiO_2	Silicon dioxide
SOI	Silicon-on-Insulator
TEM	Transmission Electron Microscopy
VOA	Variable Optical Attenuator
VSI	Vertical Scanning Interferometry
WDL	Wavelength Dependant Loss
WDM	Wavelength Division Multiplexing

SYMBOLS

C	Capacitance
d_0	Initial distance between the electrodes
E	Young's Modulus
F	Electrostatic Force
Hz	Hertz
I	Area Moment of Inertia of the beam
$K_{ES}^{i,n}$	Electrostatic spring stiffness matrix of the beam
$K_{beam}^{i,n}$	Stiffness matrix of the beam
L	Length of the Beam
$M^{i,n}$	Mass matrix of the Eigenvalue problem
m	mass of the beam per unit length
N	Newton
r	distance between the actuator and the ground electrode
R	Radius of the cylindrical actuator
T	Kinetic energy of the beam
U_{ES}	Potential energy due to the electrostatic force on the beam
U_{BEAM}	Potential energy of the beam
V	Voltage between the electrodes
w_0	Waist radius of the beam at the plane of output fiber
Y(x)	Static Deflection shape of the beam

$Y^d(x)$	Dynamic mode shape of the beam
z	Separation distance between the fibers
ε_0	Electric permittivity of air
$A^d{}_i$	Deflection coefficients
ε_r	Di electric constant of the medium between the electrodes.
δ	Lateral misalignment
ν	Velocity of the beam
η	Coupling efficiency
θ	Angular misalignment
n_o	Refractive index
ϕ_i	Boundary characteristic orthogonal polynomials
π	Total potential energy of the electrostatic actuator
ω	Natural frequency
λ	Free space wavelength

CHAPTER 1

INTRODUCTION

1.1 INTRODUCTION TO MEMS

If automation was the trend of the last century, integration is the trend of this century. Automation of physical effort, physical transport and manual computation were all seen in the 20th century. Real time control of these systems by integrating three important components of closed feedback control: sensing, electronic control and actuation is the major goal of research today. Miniaturization has been the key for this integration and MEMS (Micro electromechanical systems) evolved out of this Miniaturization. They are micromachines that use the brains of microelectronics in sensing and controlling the environment in various possible ways. The amazing closeness to the site of monitoring and accessibility to the real problem are the biggest advantages of miniaturization and this has rendered possibility of many in-situ applications like pressure and temperature monitoring in harsh environments like those found in turbines [1]. MEMS have wide applications as accelerometers and gyros in inertial measurement, ink jet printers, biometric chips and lab on a chip in micro fluidics, switches, attenuators and displays in optics, pressure measurement and RF devices. Apart from transduction they also have been used for applications like power generation. Figure 1.1 shows MEMS based radial inflow turbine designed to produce 60 watts of mechanical power at speed of 500m/sec and 2.38 million rpm [2].This shows the promising potential of MEMS. The credit for revolution of this scale goes to Silicon which is a material with amazing mechanical and optical properties, and which has also proved its best in IC and VLSI technology. The

market for MEMS is very widely expanding with commercialization of devices in various fields.

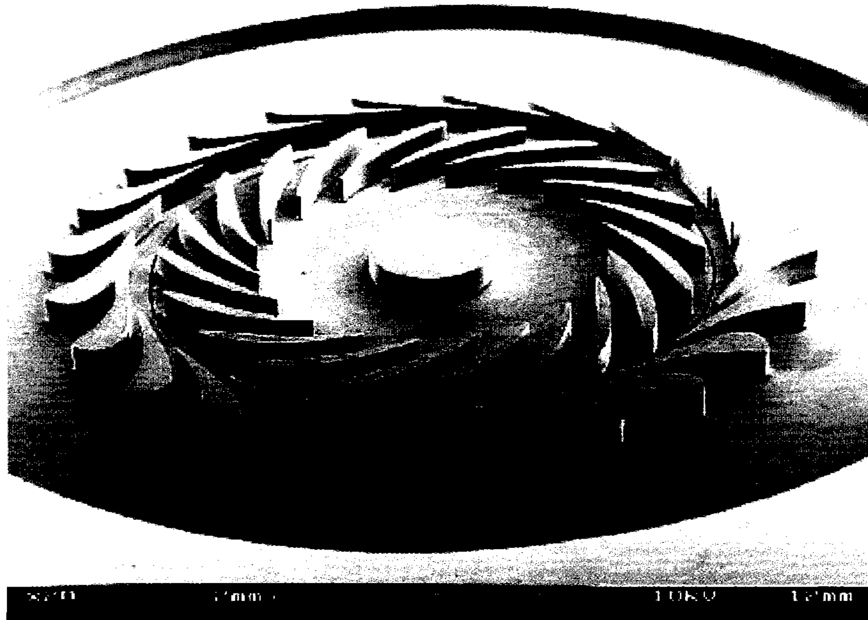

Figure 1.1: A 4:1 pressure ratio, 4 mm rotor diameter radial in flow turbine stage. [2]

MEMS integrate science, engineering and technology. The technology that drives the creation of these miniature components, devices and systems is micromachining. Any design one can conceive in MEMS is widely limited by the fabrication technology. MEMS fabrication technologies have their origins from the well established IC Fabrication process and are classified into three main categories: Surface micromachining, Bulk micromachining and LIGA technologies.

Surface micromachining is a method of fabrication that utilizes selective deposition and removal of layers one on another to finally create complex planar micro structures and devices. This is a thin film technology as each layer can have a maximum thickness of 5 microns [3]. Its compliance with ICs and use of CMOS facilities makes it the major commercial fabrication technology for MEMS. The machining in micro level is performed by chemicals rather than the use of sharp tools as in macro level and is known as etching. Bulk micromachining utilizes various etching techniques like direction independent isotropic etching, direction dependent anisotropic etching and concentration dependent etching to remove the bulk of the silicon wafer and fabricate three dimensional microstructures. The selective deposition and etching is performed using a technique called photolithography which uses a photo resist in conjunction with a mask in creating patterns on the substrates. LIGA (Lithography, Galvanoforming and molding) is another technology that can create high aspect ratio microstructures of height in the range of millimeters for making very high power and performance actuators. Both additive processes, such as, deposition, sputtering and lift off and subtractive processes, such as etching are used in combination to make tiny features. Majority of the MEMS devices are made of simple structures such as beams, cantilevers, plates and membranes. The mechanical energy needed to move these tiny devices is supplied by the actuation mechanisms.

1.2 ACTUATION

Actuation can be defined as the mechanism for energy conversion that moves the device. Currently various types of actuation exist that are based on the principles of electrostatic,

piezoelectric, thermal, shape memory alloy and magnetic actuation phenomenon. A brief introduction of the most widely used actuation methods is presented in the following section.

1.2.1 THERMAL ACTUATION

This actuation utilizes the principle of thermal expansion of a material to obtain mechanical motion. A bimorph actuator is the most widely used for out of plane actuations which uses the difference in the thermal coefficient of expansion of two materials for warping or deflecting the structure. Also asymmetric thermal actuator based on variation in geometry is used for in plane deflection. This uses the principle that thermal resistance varies with width of the cross section and hence narrow sections get heated more and creating hot and cold arms. The heat is generated often by electro thermal Joule heating due to its IC compatibility. They are popular for the very large forces and deflections that they generate.

1.2.2 PIEZOELECTRIC ACTUATION

Some materials, such as, quartz and Lead zirconate titanate (PZT) undergo deformations when subjected to electrical field and generate electric charge when deformed. This special reversible effect is called piezoelectricity and has been well exploited for sensing and actuation in MEMS. Many micro actuators have been fabricated using these materials and most of them use the stack configuration where layers of piezoelectric materials are stacked one another which generate huge deformations together under electric field. Other configurations like disk actuators and bimorph have also been demonstrated [4].

1.2.3 ELECTROMAGNETIC ACTUATION

Electromagnetic actuation is based on force generated by the magnetic field between two electromagnets of different polarity. This is a flexible mechanism as both attractive and repulsive forces can be generated. They require special fabrication techniques as they usually require coils and deposition of magnetic materials for the generation of magnetic field. They generally need constant current for their working.

1.2.4 ELECTROSTATIC ACTUATION

This makes use of the attractive forces generated between two oppositely charged conductors when a voltage is applied across them. The simple principle of operation, ease of fabrication which requires one free standing structure in space with fixed structure, low power consumption, high actuation force because of the scaling effect in micro dimensions and finally the possibility of mass fabrication due to their compatibility with existing IC fabrication technologies make electrostatic actuation, the most widely used and exploited actuation in the MEMS. Hence, more is discussed about various types of actuators that use this mechanism in the next section.

1.3 TYPES OF ELECTROSTATIC ACTUATORS

Depending on the direction of motion they are classified into in-plane and out of plane actuators.

In plane actuators move in a direction parallel to the substrate and hence have more room for movement. The most popular is the comb drive actuator. This consists of two sets of interdigitated fingers, one of which is fixed and the other connected to a movable

suspension [4]. This type of actuators always requires a suspension which is compliant in the direction of motion and stiff in the perpendicular direction. They have been widely used for many applications ranging from optical shutters and micro grippers to motors and gears.

Out of plane actuators move perpendicular to the direction of the base and are of two major types: parallel plate actuator and torsional actuator. The parallel plate actuator uses a flexible beam or plate like structure supported at edges to move in the lateral direction. The actuating force is obtained from the fixed electrode beneath the structure. Torsional actuators consist of a rigid plate or mirror that is supported on a hinge or a suspension about which the structure can rotate. The actuation can be achieved by either by electrostatic force from the ground electrode or by another comb drive actuator connected to the hinges.

Various configurations based on the different geometries of the electrodes have been proposed. Actuators using curved electrodes and multiple electrodes [5] have been proposed to cater to the different applications. For example Elata et al [6] proposed a multi electrode driven torsional adaptable micromirror whose properties could be tuned by the end user by varying the voltages for the required application.

Recently a special class of actuators that use cylindrical moving electrodes have began gaining importance. Though these electrodes cannot be fabricated by MEMS processes, the integration of fiber optics into MEMS using V grooves fabricated by micromachining and also advent of nanotubes gave rise to the possibility of using these structures as actuators for different applications like nanotube actuators, nanotweezers, optical fiber switches etc. Hence understanding their behaviour and accurate modeling of

these structures is essential for their success in applications. These structures cannot be well defined by parallel plate approximation and have to be defined considering their 3 dimensional structure and interactions with the electrostatic field. Hence modeling these kinds of structures forms the central theme of this work which will be presented in detail in the next chapters. Also this type of cylindrical electrostatic actuation has been proposed for application as variable optical attenuators (VOA) which leads us to the next section on attenuation.

1.4 ATTENUATION

In order to understand the concept of attenuation and its principles, it is important and worth while to look at the fiber optic networks in general. It is very obvious that fiber optic cables have started replacing the conventional copper and coaxial wire transmission systems and have lead to the era of fiber optic networks. The growing demand for bandwidth and faster transmission is very well driven by the internet, satellite television and other data communication industries. The higher capabilities of the fiber optic systems like high speeds in the range of gigabits, large bandwidths, ability to travel large a distance without noise has made it the popular system for telecommunications.[7]. The basic principle of all these systems is that the data to be transmitted is modulated on the optical signal in one of three ways using amplitude, wavelength and phase modulation. The term modulation is equivalent to translation as the data to be transmitted is translated by superimposing the effect of the data to be transmitted on a carrier optical wave and finally translated back to be interpreted at the receiver end. The carrier optical signal via fiber optics transmits this data through distances of thousands of kilometers and finally it is demodulated at the receiver. Also a single fiber may not carry only one data channel as

the data could be mixed in a systematic way by the process of multiplexing and finally be separated at the respective exit points. This multiplexing is performed to let all the data transmitters to share a channel at the same time leading to real time sharing. The data is actually multiplexed using certain protocol of time division, wavelength division or code division to let identify the data at the end by the process of demultiplexing.

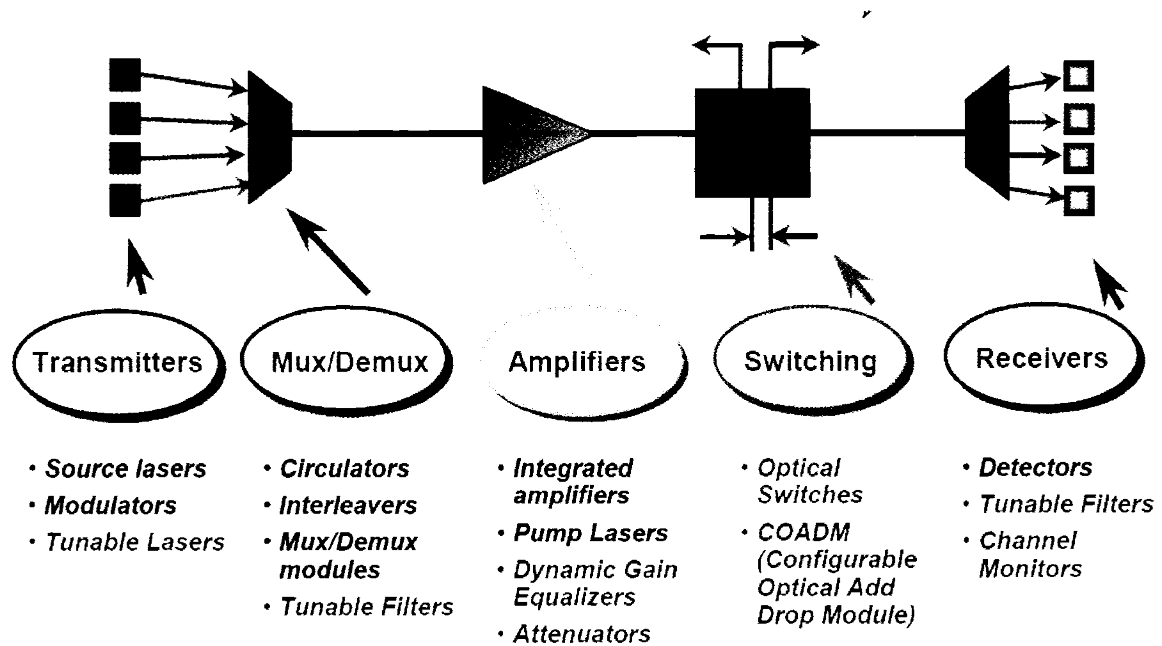

Figure 1.2: WDM network showing various components [8]

Figure 1.2 shows a typical Wavelength Division multiplexing (WDM) fiber optic network. The network consists of an array of transmitters which are a source of modulated light typically a laser or LED, a multiplexer that combines data, amplifier that boosts the signal of light and attenuators that take care of excess gains in the signals and the detector that can detect the signal at the end. MEMS started replacing the conventional devices in each of these stages of the network because of their high speed,

reliability and small size and have triggered the race for commercialization especially in switching and attenuators. Attenuators form an important class of devices that are used to control the intensity of optical signal and always ensure that the intensity is within the maximum value of the dynamic range of the detector. They are very vital as there are various sources of variation of the signal in the optical network which when left uncorrected can result in huge bit error rate of the data transmitted. Variable optical attenuators (VOA) are tunable optical attenuators that provide continuous range of attenuation and are a very important class of active photonics components that control in real time. They are used throughout the optical network and are typically placed after transmitters to provide gain equalization in channels of different wavelengths, after optical amplifiers, and before the receivers for signal attenuation to prevent detector saturation [9]. Study of these VOAs forms major component of this thesis and hence the principle of attenuation and types of attenuators will be presented in the next sections.

1.5 TYPES OF ATTENUATION

As already described, attenuation is the process of controlled reduction or loss of the intensity of optical beam to desired levels. This can be achieved either by manipulating the optical beam within the waveguide or outside the waveguide. This has led to two types of attenuation schemes: waveguide based attenuation scheme and non-waveguide based attenuation.

1.5.1 NON-WAVEGUIDE ATTENUATION SCHEMES

This type of attenuation is generally achieved by manipulating the optical beam during its free space propagation through some kind of mechanical interference. Two major categories in these are shutter based VOAs and Mirror based VOAs. The former type introduces a mechanical stop called shutter in the line of the light beam to partially block the light. They are all called transmission type VOAs and are very simple in operation. Various actuation mechanisms including electrostatic [10], [11], [12], electromagnetic [13] and thermal [14] actuations have been used to make these kinds of VOAs. Electrostatic actuation is widely used because of its ability to obtain higher actuation and mostly comb drive actuators have been used. Thermal actuation based VOAs traditionally employ thermally actuated to achieve the attenuation. Also the way in which these shutters pop up in the optical line have led to different types of attenuators like in plane, out of plane attenuators [15], [16]. Also a scratch drive actuator that uses a residual stress-induced flexure curved beam with corrugated trench anchors that can lift up the reflective mirror shutter has been proposed by Chengkuon lee [17]. Most of them have to use metal coatings on the side walls of the vertical shutters which are not optically flat and they suffer from the problem of edge scattering that adds an additional uncontrollable component of optical loss. Devices with dual or multiple shutters have been used to have predictable wavelength loss based on the principle that peak of the far field diffraction pattern obtained when the beam passes through the shutter has to be on axis. R.RA. Syms et al [18] proposed a sliding blade MEMS iris VOA that uses multi shutters to achieve this. The VOA is named iris as it is similar to the pupils in the eyes that control the aperture. Figure 1.3 shows a typical electrostatic actuator driven dual

shutter mechanism with the fibers not installed [19]. They achieved an attenuation range as high as 57 dB, though it had return loss of around 37 dB. They also demonstrated a simple packaged and pigtailed chip with an array of four attenuators.

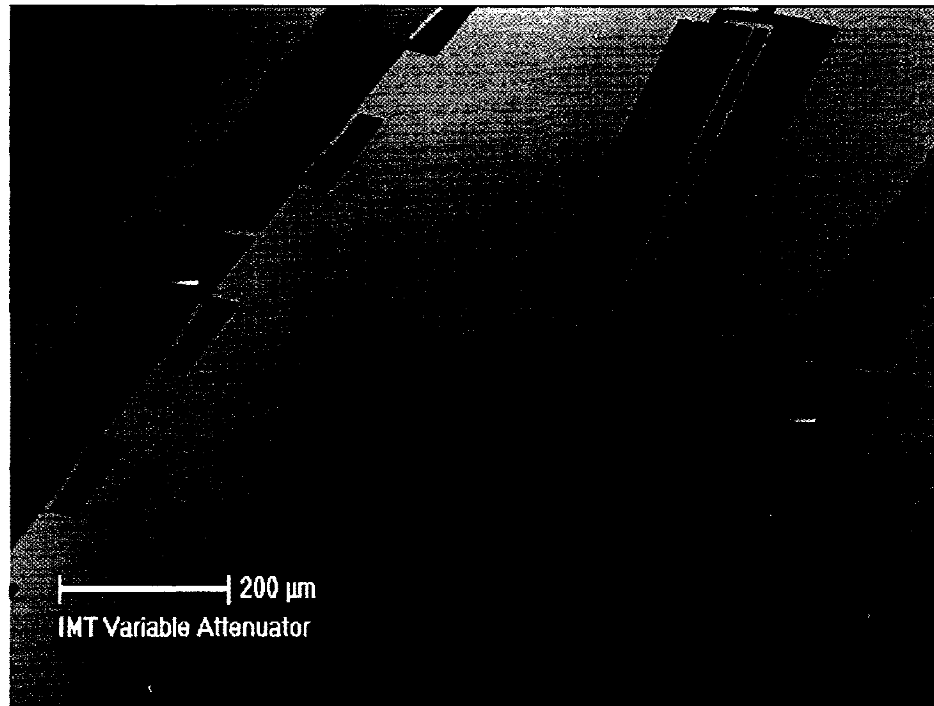

Figure 1.3: Scanning electron micrograph of a dual shutter attenuator driven by a comb drive [19]

The other type of attenuation is performed by manipulating a reflective mirror and its angle of tilt to change the orientation of the output signal and there by creating misalignment. This eliminates the loss due to the effect of rough edges as the light is always reflected from the flat front surface and not the edges. Changheon ji et al [20] in their work fabricated an electromagnetically actuated VOA of a maximum attenuation of 82 dB at actuation current of 43 mA. But this cannot yield lower step actuation and is very hard to control as it was highly nonlinear.

This type of attenuators is based on physically moving a reflective surface like a mirror against the path of the light. There are many variations based on the geometries of the mirror, the ways of aligning the waveguides in relation to each other and the kind of actuation used in actually achieving them and finally the number of reflections and the type of the reflection. Some use collimating optics and introduce mechanical stops in this region. This leads to magnification of the actuation in the order of 10 [4]. Kim et al proposed a variant of this mirror attenuation by using two mirrors instead of one. They demonstrated the feasibility of translation of single and dual 45 degree tilted vertical mirrors in achieving attenuations to a range of 20 dB. The major advantage of this dual reflection is the minimization of back reflection which contributes to the insertion loss. The fabrication method using lift off and micromachining has been very well demonstrated [21]. Figure 1.4 shows another variant known as a retro VOA which employs the principle of dual reflection by mirrors placed coaxially in line and with input and output waveguides parallel to each other which are not yet inserted in the trenches. The mirrors are moved in-plane by comb drive actuators and their physical translation leads to the shift of reflected light and thus creating attenuation [22].

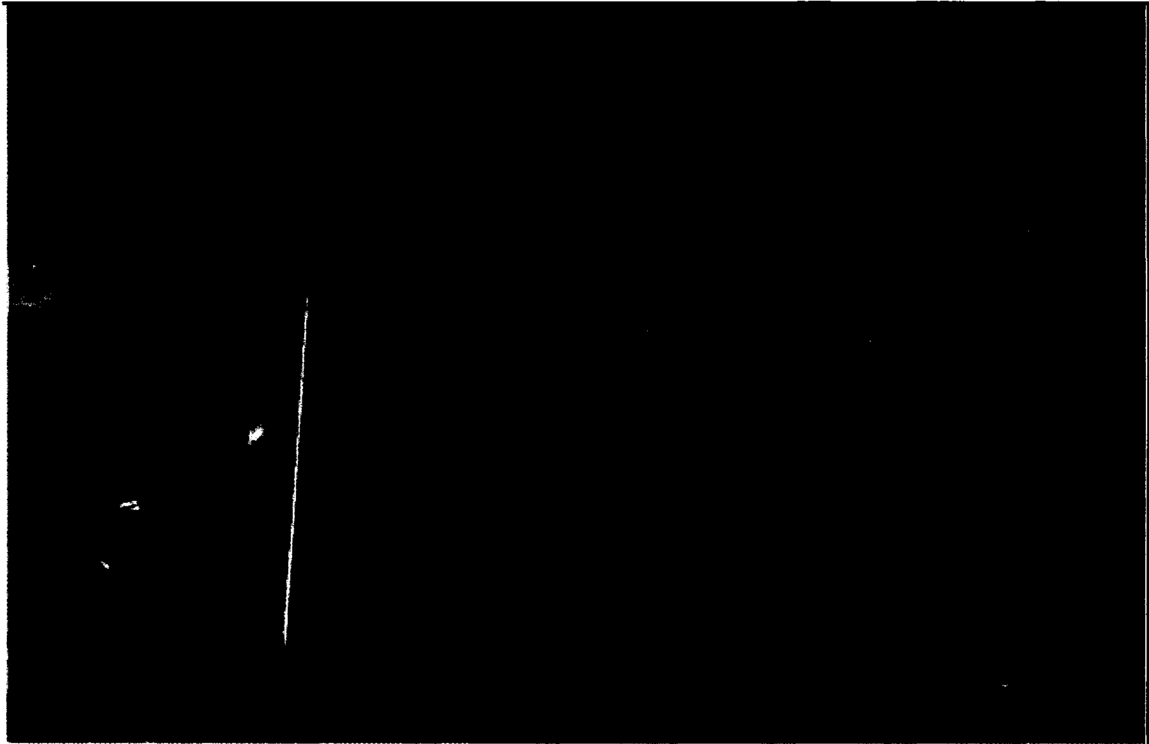

Figure 1.4: SEM image of a Retro VOA using two coaxial mirrors driven by comb drives [22].

Another interesting type of attenuator is a MARS (Mechanically-active anti-reflection switch) micromechanical modulator which is shown in Figure 1.5, is based on the principle of Mach Zehnder interferometry. This uses an anti reflecting silicon nitride film of quarter wavelength thickness suspended as a membrane and which when deflected by the same distance as its thickness would act as a reflector. The transition between this reflecting and absorbing stage has been used to control the intensity of light that is transmitted to the output waveguide. This motion and transition has been achieved by electrostatic actuation with 3 microsecond response [23].

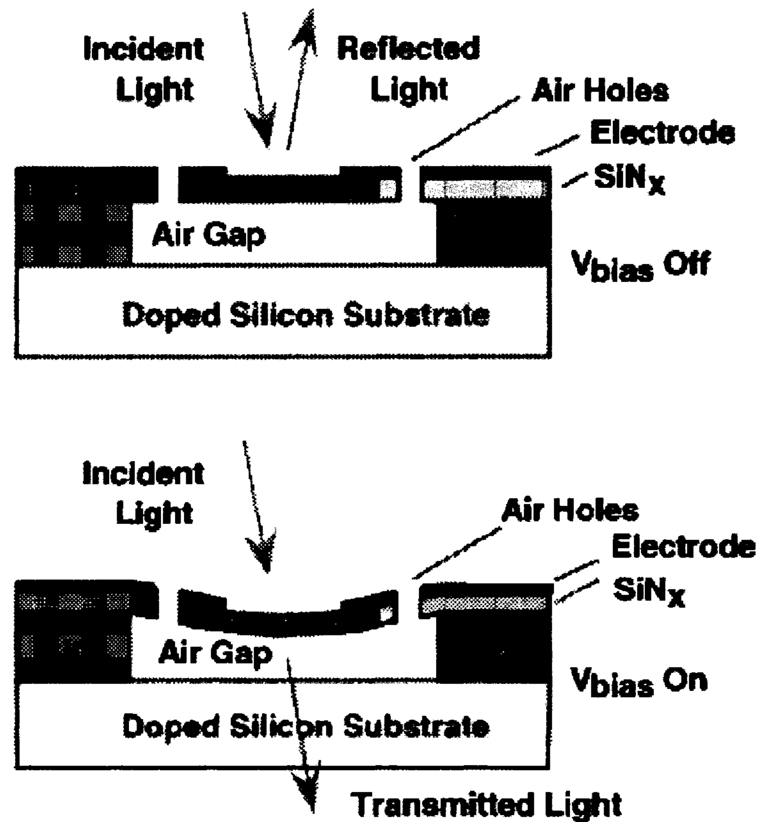

(a)

Figure 1.5: MARS type modulator based on Mach Zehnder interferometry showing both phases of attenuation [23].

Another interesting approach used by researchers is of a latching VOA where the attenuator could be fixed at each step of its operation and thus eliminating the vibration sensitivity of the device. RRA Syms et al [24] demonstrated a multistate latching VOA using rack and pinion mechanism driven by electro thermal actuators and fabricated on bonded silicon on insulator material to fix the optical shutter at a particular position. This means that the VOA has the ability to retain a desired value of attenuation without the provision of electrical power. The major advantage of all these attenuators is the large amount of attenuation achieved but the higher losses like PDL (polarization dependent

loss) and WDL (wavelength dependent loss) they exhibit can be an important issue in certain applications. Also their design and fabrication are very complex as can be seen from the Figure 1.4.

1.5.2 WAVEGUIDE ATTENUATION

The waveguide-based VOA is noticed by its large-scale integration and mass production. There are both mechanical and non mechanical types of VOAs in this category. Non mechanical types try manipulating the core or the cladding properties of the wave guide and achieve the attenuation using various losses of waveguides like dispersion, absorption and evanescence. They generally rely on varying the refractive index of the core and clad either by electro optic, thermo optic and acousto optic [25] modulation.

Electro optic modulation attenuators vary the optical properties of the clad by inducing electric field on certain length of these waveguides. Recently Electro optic ceramic materials like PLZT (Lead-Lanthanum-Zirconate-Titanate) have been proposed by Choi et al [26] for excellent response times of few micro seconds and high optical performance. Thermo optic attenuators use the relation between refractive index of the clad and temperature in varying the optical properties and thereby achieve attenuation through dispersion. A few configurations of VOAs using thermo optical switching have been proposed, ranging from straight waveguide geometries, Y-junctions and S-bends. An example is S waveguide attenuator which uses S type bend on the waveguide which is current interacted to vary the refractive index [27]. Because of their high thermal conductivity and easy integration to silicon based structures, Polymers have gained importance for application of VOAS. T.C. Kowalczyk et al [9] in their work have demonstrated a polymer VOA based on thermo optic modulation that has a resistive

heater element fabricated on the top cladding layer and placed above an embedded channel waveguide spanning a length of 1 mm. They used a stable gemfire polymer for a portion of the cladding and achieved dynamic range of 30 dB with a very low power of 10mW. This low power consumption is one of the main advantages of polymeric VOAs [28]. There is another widely used technique of attenuation which uses doping the clad or the core to create changes in optical properties. But the attenuation is generally not uniform and has bandwidth limitations. Recently Wonk young Lee et al [29] have developed a technique by doping both the core and clad with cobalt and achieved uniform attenuation from 1.25 to 1.6 microns of wavelength.

Liquid crystals also gained importance as materials for doping because of their excellent electrical response. Armen Zohrabyan et al [30] proposed an in-fiber variable optical attenuation with ultra-low electrical power consumption that replaces the silicon clad with a LC (liquid crystal) material and uses the application of electrical current in modifying the clad properties to achieve attenuation. This is an evanescent type modulation VOA that uses controlled guidance and leakage of light into clad form the core. This uses the Frederickz effect that varies the molecular orientation of the LCs by applying an electric voltage. They demonstrated very low power consumption in the range of micro watts for their design [30].The advantage of these methods is that the waveguides could be very close to each unlike shutter methods and this result in low insertion loss.

Mechanical VOAs move the waveguide by some actuation and thus achieve attenuation. Their simplicity and their ease of operation make them a favored method among VOAs. They use off alignment and geometric manipulation in achieving

the attenuation and hence most of them are wavelength independent as they do not rely on material property variations. Hence such systems have begun importance in DWDMS (Dense wavelength division multiplexing systems) where wavelength independence is a requirement for multi channel equalization.

Both 2d planar waveguides and 3d cylindrical waveguides have been used for the attenuation. The major advantage of the cylindrical waveguide or fiber type attenuation is their easy integration into the V grooves and their compatibility to the transmission fibers in the existing optical networks. This thesis proposes a cylindrical waveguide attenuation that uses the technique of misalignment. This principle of misalignment has been already used for making optical switches and aligners [31] where there are only two active states on and off. An example is a fiber switch proposed by Y.J.Yang et al [32] in their work on capacitance based actuator This employs a mechanism of moving the fiber holding table and thereby creating the fiber misalignment. This design uses comb drive actuator and folded beam suspensions in the design and has a switching response of 3.5 ms This thesis uses similar idea of misalignment for the application of continuous range of attenuation by direct actuation of the fiber and not the fiber holder thereby creating more accurate control of the device. This uses electrostatic actuation and attempts to prove the feasibility of this idea for a simple, novel and efficient VOA. The major advantage of this VOA is that since the attenuation is based on geometrical effect and not the materials the WDL is minimum. Also there is no need for any extra optics to be placed in the structure. The losses associated with free space propagation can be minimized as both the fibers can be placed at a very close distance. The details of the scheme and the other components of the thesis will be presented and

discussed in the next sections and this leads us to rationale and scope of the present thesis work.

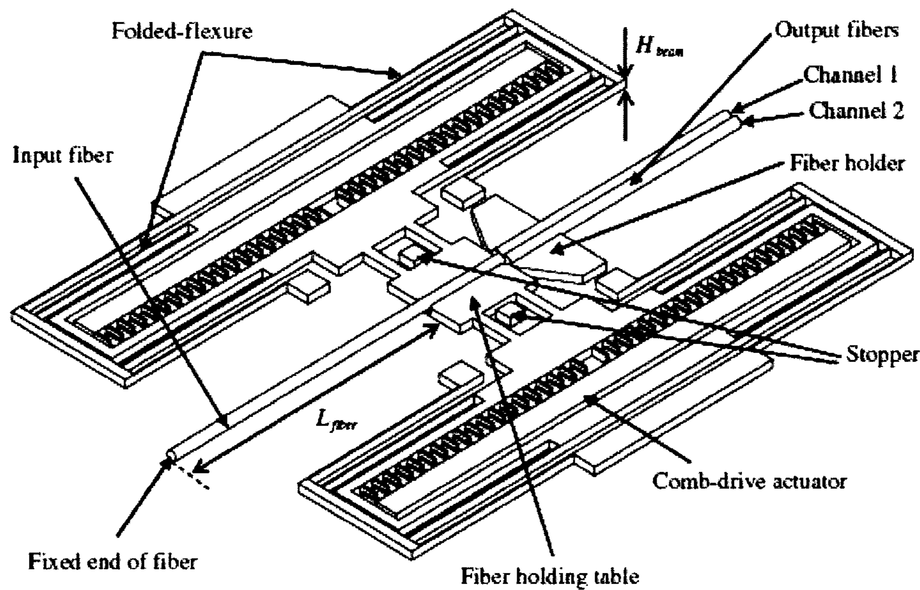

Figure 1.6: A fiber actuated optical switch by a comb drive [32].

1.6 RATIONALE AND OBJECTIVE OF THE THESIS

As already explained in the previous section cylindrical electrostatic actuators are being widely used for various applications in MEMS. The static and dynamic behaviour of these actuators form the major component in their design for their respective applications. The different physics domains involved in the actuation has to be taken into consideration using a coupled modeling approach. Modeling the electromechanical structures considering their geometry into consideration and nonlinearities and the pull in phenomenon is very important for the design of the structures. This thesis attempts to propose a generic model that describes the behaviour of such cylindrical electrostatic

actuators under applied voltages. Also Dynamic modeling is also performed to completely characterize their behaviour for dynamic conditions and eventually in calculating their response. The thesis has two main objectives

1. To develop a synthesis procedure for the design of circular actuators in general.
2. To propose a novel scheme of variable optical attenuation using circular actuators and prove its feasibility for telecommunication applications.

1.7 ORGANIZATION AND LAYOUT OF THE THESIS

The thesis is organized as follows. In general every chapter starts with an introduction and literature for the concerned chapter and ends with the summary outlining the achievements in the chapter.

1 Modeling of the individual electric and mechanical domains of the cylindrical shaped electrostatic actuation is presented in Chapter 2. Also coupled non linear static modeling and analysis of the actuator using energy methods is presented. Finally, the preliminary validation using data from the literature is presented.

2 Dynamic modeling using Rayleigh Ritz energy method and Gram Schmidt orthogonolization procedure is presented in Chapter 3. A unique boundary conditioning approach by approximating the nonlinear electrostatic force as an elastic foundation has been presented. Finally the model has been demonstrated on a carbon nanotube resonator.

3 A novel optical attenuation scheme using the actuation principle in Chapter 4 is proposed. Optical modeling of the system using Gaussian beam theory has been presented. Parametric analysis of the attenuators has been presented by varying the identified geometric and process parameters.

4 Experimental testing to validate the proposed theoretical models and design is presented in Chapter 5. Static testing using visual microscopy and dynamic testing using the principle of Laser Doppler Velocimetry are Presented and the test results are compared with the results from the designs.

5 The Chapter 6 presents the conclusion of the thesis by highlighting the major achievements of the thesis and the scope for possible future work in this area.

CHAPTER 2

STATIC MODELING AND ANALYSYS

2.1 INTRODUCTION TO MEMS MODELING

Design of MEMS needs an in-depth understanding of the behaviour of devices. There is an immense need for modeling the system to clearly understand the behaviour of the system as the same knowledge can be used to study, analyze, proactively control the system and thereby design it for the required specifications. Models also allow the effects of time and space to be scaled, extraction of properties and hence simplification, to retain only those details relevant to the problem. The Figure 2.1 displays a comprehensive list of modeling options available to engineers [33]. Most of the MEMS devices use mechanistic mathematical models for their design and synthesis as much of the system behavior can be well described by the existing theories in literature. Modeling MEMS involves three components: Simplified Description of the device and the physics behind it using consistent theory and reasonable assumptions, formulation of mathematical models to quantitatively describe the model and its behaviour in terms of differential or algebraic equations and the use of exact or relevant numerical mathematical methods to solve for the specific boundary conditions and initial conditions [34]. Mostly Continuum mechanics is used for the description of motion of these micro scale objects still on a macro scale. MEMS always involve multi physics domains and hence the modeling method used is dictated mostly by the actuation mechanism used.

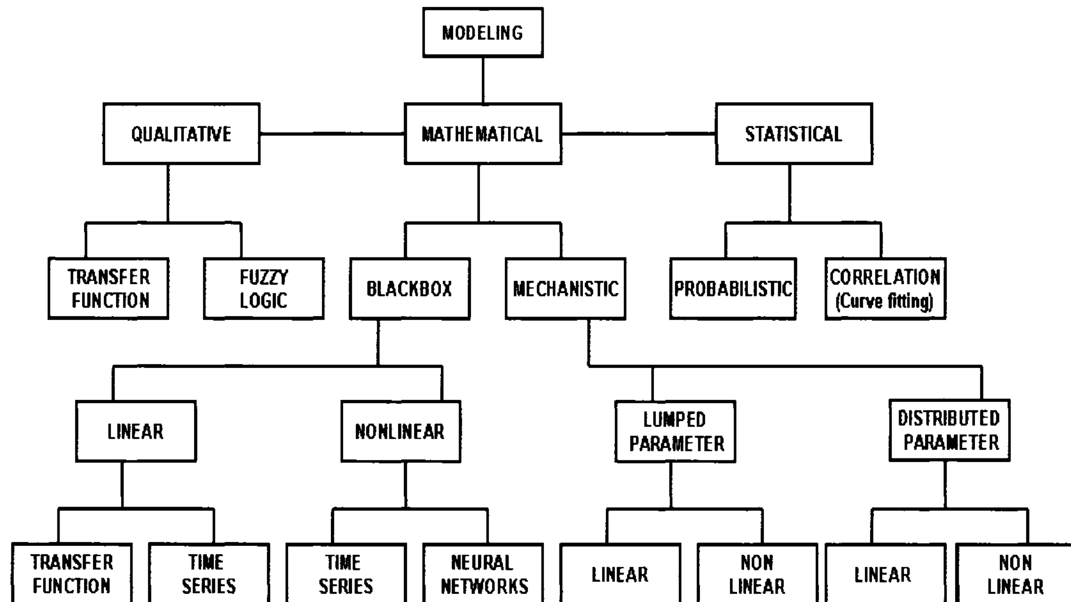

Figure 2.1: Block diagram showing the modeling tools often used in mechanical product design

2.2 MODELING ELECTROSTATIC ACTUATION

The principle of electrostatic actuation can be best explained in simple by parallel plate actuation shown in the Figure 2.2. When a bias voltage is applied between two parallel electrodes, charges are induced on the electrodes. This creates an electrostatic force which displaces the free electrode. The force generated by this voltage is defined by Coulombs famous inverse square law and is given by the Equation (2.1),

$$F = \frac{\varepsilon_0 \varepsilon_r A V^2}{d^2} \qquad (2.1)$$

where,

F- Electrostatic force

ε_0 - Electric permittivity of vacuum, 8.85 * 10^{-12}

ε_r - Dielectric constant

A – Overlapping area of the electrodes

V- Bias voltage applied

d- Distance between the electrodes.

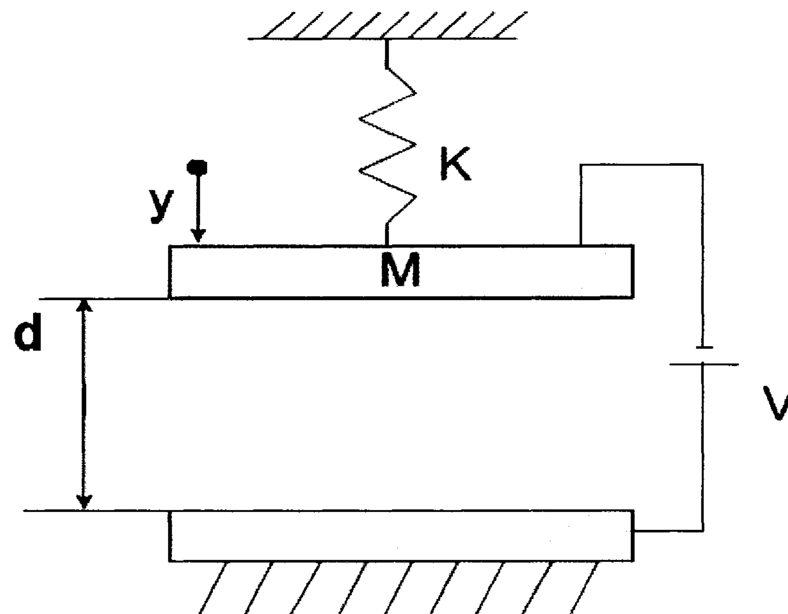

Figure 2.2: Schematic of parallel plate actuation

The model shown in the figure is a typical lumped model used for understanding the static behaviour of an actuator. This simplified representation is very representative of the mode of operation of micro-systems such as micro-actuators and micro-accelerometers. The mechanical structure is modeled as a combination of a rigid lumped mass and a spring of equivalent stiffness that describes the device. Most of the structures are complex and continuous and hence distributed mass models have to be considered for accurate results.

Modeling of the electrostatic actuation involves solving the electrostatic forces generated due to the voltages applied and thereby the displacements of the actuator. Many models are pervasive in the literature; that predict these actuators. Approaches vary from very rough approximations based on combinations of parallel plate capacitor elements, analytical or numerical Schwarz–Christoffel (SC) conformal mapping-based techniques [35], and numerical solutions of the electrostatic field equations. Powerful numerical approaches are very accurate, but laborious and time-consuming, while simple approaches are inaccurate. Though the specifications of the exact model employed depend on the geometry, boundaries and the structures used, in general, all these models have certain major concerns given below:

1. non linearity
2. electromechanical coupling.
3. pull in
4. residual charge

2.2.1 NONLINEARITY

Nonlinearity is inherent characteristic of any electrostatic actuator. This nonlinearity is mainly due to the electrostatic force being nonlinear with the deformation. Many models in literature have used some kind of approximation like Taylors series to linearise the model for the solution [36]. The other source of nonlinearity is from the large deflections of the cantilever where the isotropic linear approximation no longer holds good and leads to great deviation in results.. The trade off between accuracy and speed and ease of computation is a major criterion in selecting the linear or the nonlinear analysis of beams. Gang li et al [37] in their work analyzed the importance of nonlinear approach compared

to the linear and found the criterion where the nonlinearity can be neglected. They found out from their analysis that for a particular cantilever beam if the electrode gap to length ratio is less than 20 percent the nonlinear approximation can be relaxed as it gives the same accuracy as the linear one. They also came up with a mixed regime approach which uses a combination of both methods, linear at low voltages and nonlinear at higher voltages.

2.2.2 ELECTROMECHANICAL COUPLING

When a dc voltage is applied to the actuator at rest, it induces charges on the surface of the moving electrode that in turn induce a normal electrostatic force over the same electrode. This electrostatic force causes the mechanical flexible structure to deform and will lead to a reorganization of the surface charges. This causes further deformation and this is considered as coupled electro-mechanical behavior. Accurate modeling and design of the electrostatic MEMS needs strict consideration of the strong coupling that exists between the electrical and mechanical fields. Several advanced numerical methodologies have been proposed and implemented in the literature to deal with the multiphysics coupling and simulation for various electrostatic actuation schemes. Major literature have compared the problem of electromechanical coupling in electrostatic actuation to a similar coupling of pressure and velocity in incompressible fluid flows and applied similar methods. There are two major approaches that deal with the electromechanical coupling, a direct method that considers both the electrical and mechanical domains simultaneously and the sequential or the relaxation method which considers each domain sequentially in a series of iterations. In the first method, a potential function consisting of both electrical and mechanical energies is formulated and it is minimized using energy

methods and finally solved for the deflection of the actuator [38]. This is more accurate but has to be carefully formulated for complex geometries. The sequential method transforms this coupled problem to a series of uncoupled problems by using method of iteration [39]. At each sub step the electrostatic force is calculated and the load is transferred to the mechanical model to compute the structural deflections and then again the forces are computed corresponding to the new deformations. Convergence is a major problem using this approach for complicated geometries. The flexibility of this method makes it the preferred method in Commercial MEMS CAD software [40]. Boundary element methods are used often in the analysis of exterior electrostatics problems as it requires only meshing of a surface and not a volume which eases the computation time and effort while Finite element methods describe the volume of the structure [41].

2.2.3 PULL-IN PHENOMENON

It can be seen from Equation (2.1) that when the applied voltage increases the electrodes come closer together. When a critical voltage is achieved, the electric force becomes dominant with respect to the mechanical force and the electrodes touch down. This critical voltage is called the static pull-in voltage. The modeling of this pull-in is very important as this limits the operation of any electrostatic actuator and is also the useful phenomenon in the case of bistable switches where pull-in or touching down of the electrode is a part of its operation. The analytical expressions of the pull-in voltage for a parallel plate actuator as a function of stiffness k and gap d_0 is given by [42],

$$V_{pi} = \sqrt{\frac{8kd_0^3}{27\varepsilon_0\varepsilon_r A}} \tag{2.2}$$

Where

K –Equivalent mechanical stiffness

d_0 – Initial electrode gap

A – Overlapping electrode area

ε_0 - Electric permittivity of vacuum, 8.85 * 10^{-12} f /m

ε_r - Dielectric constant

2.2.4 RESIDUAL CHARGES

The effect of residual charge that can accumulate in electrostatic actuators containing electrical insulators in contact with the conductors has been considered by Rochus et al [43] by assuming an auxiliary charge at the interface of the dielectric layer and air. They expressed the energy expression as a complementary to the electrostatic potential energy as given by the Equation (2.3),

$$U_{Res} = \frac{Q_{Res}^2}{2(C_x + C_d)} \tag{2.3}$$

where

Q_{Res} is the residual charge on the insulator

C_d is the dielectric capacitance separating the electrodes.

C_x is the capacitance of the actuator configuration.

The effects of the force of gravity on these microstructures can almost always be ignored except for applications like high sensitive accelerometers [42].

When there is a network or array of capacitors in action, the fields can be overlapping and can cross influence the pull-in limits and even the basic static deflections. Electrostatic models that use conformal methods have also been proposed by Robert Bosch [44]. Secondary effects such as Coulomb friction, hysterisis and eddy currents are mostly neglected. Apart from these major influences, literature also considered various geometries of both moving electrodes and flat electrodes. Not much has been done in the modeling of cylindrical MEMS. Since the advent of nanotubes and fiber actuators, modeling of them has become a topic of interest and hence this thesis attempts to model this scheme and is demonstrated for various applications. Nonlinearity due to large deformations is neglected in this work since the gap electrode ratio is always less than 20 percent for all the actuators considered through out the thesis. Nonlinearity due to electromechanical coupling is considered and solved by a direct iteration approach. Each of the domains has to be described by the respective theories and the coupled problem will be solved in the next sections.

2.3 ELECTROSTATIC MODELING OF THE SYSTEM

The electrostatic model calculates the electrostatic force induced on the movable actuator when a bias voltage is applied between the top and the lower electrode. The Figure 2.3 gives the schematic of the principle of electrostatic actuation scheme used in the thesis. As can be seen the cylindrical actuator has a completely different electric field. The field is always normal to surface of the two electrodes. The electric field lines start normal to the cylindrical curvature at every point and perpendicular to the flat straight electrode at

the bottom as can be seen from the Figure 2.3, Hence the crawler shape of the electric field can be noticed. The cylindrical waveguide or actuator is assumed to be a continuous line charge for the purpose of the computation of electrostatic charges on the surface using Gauss law. Method of images is a classical problem solving tool in electrostatics that replicates the boundary conditions of the problem layout using a mirror of imaginary charges that is used here.

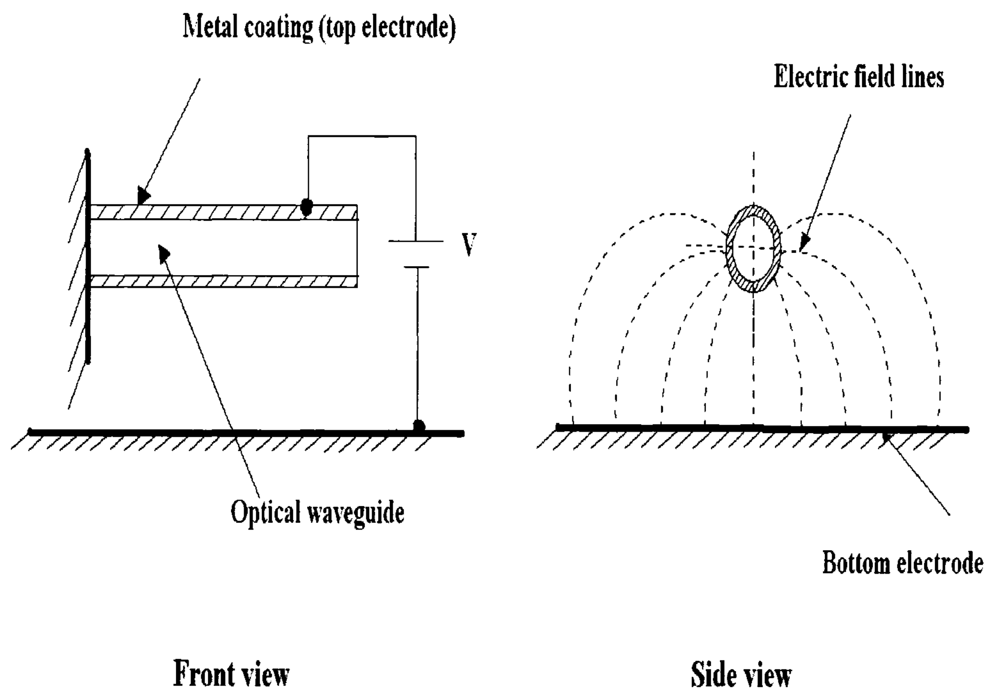

Figure 2.3: Schematic showing the electric fields induced on a cylindrical electrostatic actuator

The voltage is assumed to be constant throughout the length. When the cylindrical actuator deforms and displaces, it is no longer parallel to the ground electrode and also the distances vary from the tip to the fixed end. Hence, the theory can no longer be fully accurate. So as to cater to the real situation, the model is modified by means of discretization over the entire length using continuous functions. The cylinder is assumed

to be a series of infinite cylindrical discs of elemental thickness 'dx' and each is parallel to the ground plane having a separation given by the position variable x given by r(x). Hence, the capacitance per unit length for the cylindrical fiber over the conductive ground electrode is given by [45],

$$C(x) = \frac{\pi \varepsilon_0 \varepsilon_r}{\log\left[1 + \frac{r(x)}{R} + \sqrt{(1 + \frac{r(x)}{R})^2 - 1}\right]} \qquad (2.4)$$

where R is the radius of the cylindrical actuator, r(x) is the gap between the cantilever fiber waveguide and the ground plane, ε_0 is the permittivity of air gap between the electrodes and ε_r is the dielectric constant of the medium between the electrodes.

The value of r equals d_0 when the moving waveguide is un-deflected, d_0 is the initial undeflected gap between moving waveguide and bottom electrode. The gap variation with the position variable x can be defined as,

$$r(x) = d_0 - Y(x) \qquad (2.5)$$

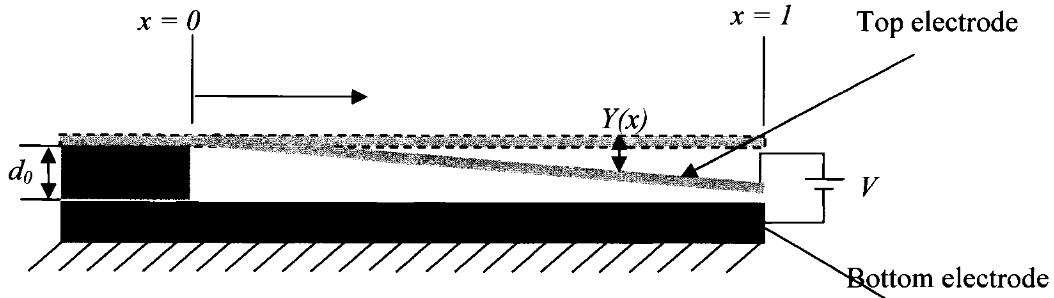

Figure 2.4: Schematic showing the deflected electrostatic actuator.

2.4 MECHANICAL MODEL OF THE SYSTEM

The mechanical model describes the moving structure of the system which in this case is the top electrode. Euler-Bernoulli beam theory which is a simplification of the linear isotropic theory of elasticity is used in the modeling of the structural deformations as the materials that constitute the actuators used in the modeling through out the thesis are linearly isotropic. The following assumptions are used throughout the modeling. The actuator is assumed to be an Euler beam. Axial effects like stretching and torsion are neglected. Theory of pure bending is used. According to this theory, the mechanical energy or the strain energy of the beam is given as,

$$\mathrm{Ubeam} = \frac{1}{2}\frac{EI}{L^3}\int_0^1 \left(\frac{d^2Y(x)}{dx^2}\right)^2 dx \tag{2.6}$$

where E is the Young's modulus of the beam, $Y(x)$ is the deflection of the beam as a function of the normalized position variable x, I is the area moment of inertia of the circular cross-section and L is the length of the beam which is shown in Figure 2.4.

2.5 COUPLED ELECTROMECHANICAL MODEL AND SOLUTION

Rayleigh's method of variational calculus is used in solving the coupled multi domain problem. This is just the principle of minimum total potential energy derived as a special case of the virtual work principle for elastic systems subject to conservative forces. According to the principle of virtual work or the principle of stationary energy [46], the

total potential energy of a system is a local minimum at its stable equilibrium state presented by,

$$\delta\pi = 0 \tag{2.7}$$

where

The total potential energy, π, is the sum of two terms, the elastic strain energy stored in the deformed body and the potential energy of the applied forces. The applied forces in this case are the electrostatic force acting over the entire beam and hence the second term equals the electrostatic energy of the system because of the induced electric field.

$$\pi = \text{Ubeam} - \text{Uelec} \tag{2.8}$$

Substituting Equation 2.8 in Equation 2.7 we arrive at

$$\frac{d\text{Ubeam}}{dY} - \frac{d\text{Uelec}}{dY} = 0 \tag{2.9}$$

$$F_{ES} = \frac{d\text{Uelec}}{dY} = \int_0^1 - \frac{\pi\varepsilon_0\varepsilon_r V^2 L}{R\sqrt{\frac{r(x)(r(x)+2R)}{R^2}}\log^2\left[1+\frac{r(x)}{R}+\sqrt{\frac{r(x)(r(x)+2R)}{R^2}}\right]}\,dx \tag{2.10}$$

$$\text{Ubeam} = \frac{1}{2}\frac{d[\frac{EI}{L^3}\int_0^1\left(\frac{d^2Y(x)}{dx^2}\right)^2]}{dY} \tag{2.11}$$

Solving this equation using exact methods analytically is impossible and hence an approximated spectral numerical method called Rayleigh method is used. According to

this method the deflection shape is approximated as summation of N basis functions. Each of these functions has to satisfy at least the essential boundary conditions to fit the boundary of the problem and eventually the solution. The deflection shape Y(x) is assumed to be a set of basis functions ϕ_i which satisfy at least the essential boundary conditions given as,

$$Y(x) = \sum_{i=1}^{n} A_i \phi_i(x) \tag{2.12}$$

Substituting this assumed deformation in all the energy terms in the above equations, will result in solving of these coefficients. Hence, static deflection shape is thus obtained by minimizing the total potential energy π as given by,

$$\frac{d\pi}{dA_i} = 0 \tag{2.13}$$

Therefore, from Equation (2.8) we can write,

$$\frac{dUbeam}{dA_i} - \frac{dUelec}{dA_i} = 0 \tag{2.14}$$

Where $\frac{dUelec}{dA_i}$ can be reduced to

$$\frac{dUelec}{dA_i} = \int_0^1 \frac{\pi\varepsilon_0 V^2 \phi_i L}{R\sqrt{\frac{r(x)(r(x)+2R)}{R^2}}\log^2\left[1+\frac{r(x)}{R}+\sqrt{\frac{r(x)(r(x)+2R)}{R^2}}\right]} dx \tag{2.15}$$

First term of Equation (2.14) is the equivalent mechanical force from the beam which is linear and the second term is the electrostatic force which is non linear. Solving this

governing non linear equation is not possible analytically and hence it is to be solved numerically to compute the deflected equilibrium shape of the fiber. Both the electrostatic and the mechanical beam forces are computed for various assumed deflection coefficients and are plotted with the deflection in Figure 2.5. The two computed mechanical and electrical curves have two points of intersection, the first corresponding to the stable equilibrium and the second corresponding to the snap equilibrium. Thus, the deflection coefficients and thereby deflection shapes are evaluated from the points corresponding to stable equilibrium shown in Figure 2.5 for a 15mm silica waveguide having electrode gap of 30 microns. The dimensions and properties used for the model are given in Table 2.1.

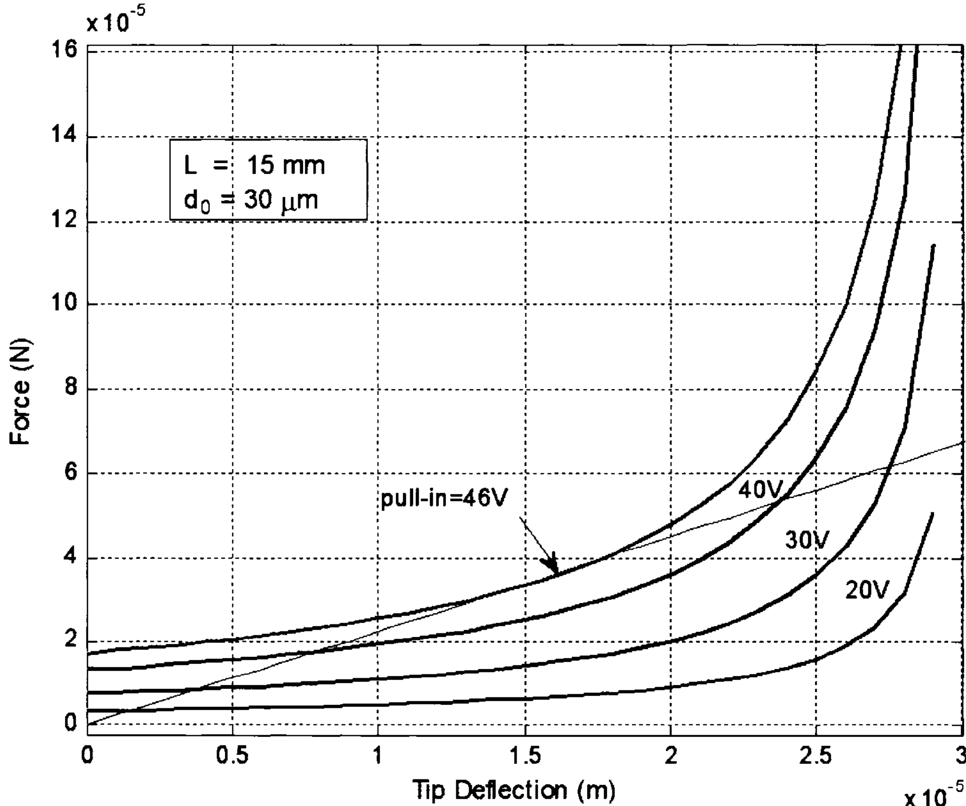

Figure 2.5: Linear mechanical force and nonlinear electrostatic forces evaluated for various voltages

Table 2.1: Properties of the silica cylindrical waveguides used for static analysis.

Length of waveguide	15 mm
Diameter	125 μm
Electrode gap	30 μm
Youngs modulus	66 GPa
Electric permittivity (air)	1

Figure 2.5 shows a typical plot of electrostatic force at various voltages versus the linear mechanical restoring force. It can be seen that each electrostatic force has two points of intersection. The first point of intersection between the electrostatic and the mechanical force gives the stable equilibrium and the corresponding deflection of the actuation at that particular voltage. The second point of intersection corresponds to the unstable equilibrium of the actuation. This is the same as the pull in point mentioned in the previous section where the electrostatic force dominates the mechanical force and the actuator yields to it touching the bottom electrode. Also a third point of intersection has been reported in literature [47] especially in torsional electrostatic actuators where there is a significant effect of counter electrostatic force coming from the top surface of the moving electrode. This is normally not to be seen in beam actuation as the counter field is very negligible. Also it can be seen that beyond certain value of the applied bias voltage the two points of intersection converge to one point. At this point the linear mechanical force becomes tangent to the electrostatic curve at that voltage. This is known as the static pull-in condition and beyond this point any voltage applied leads to

the snap down of the actuator. This cutoff voltage is known as the static pull-in voltage of the actuator and the distance between the tip of the device and the ground electrode at this cut off point is known as the pull in distance. It has been widely reported in literature that this pull in distance is normally one third of the initial distance between the two electrodes for the scheme of parallel actuation [48]. But from the Figure 2.5 it can be very well seen that the pull in distance is close to one half of the initial electrode gap. This can be accounted to cylindrical actuation and the curvature of the actuator. The bottom part of the cylinder is just a line edge and the field is low compared to a parallel plate actuator. The instant the longitudinal section with equivalent area as a parallel plate actuator reaches the one third pull in point; the line edge already reaches the one half distance of the electrode gap. This one is a very interesting inference and observation from the analysis of the cylindrical electrostatic actuation.

2.6 VALIDATION OF THE MODEL

The model has been validated by comparing with a similar cylindrical actuator but in nano scale. The modeling is still valid and can be applied to the nano actuator in the reference because the diameter to gap aspect ratio is still high. The following Table 2.2 lists the parameters and dimensions that are used in the computation of the tip deflection of the nano actuator. The nano actuator considered is a hollow double wall nanotube and its moment of inertia is obtained by the Equation (2.16),

$$I = \frac{\pi}{4}(R_{out}^4 - R_{in}^4) \qquad (2.16)$$

Where R_{out} and R_{in} are the outside and inside diameters of the nanotube respectively.

Table 2.2: Properties and dimensions of the nano actuator used for theoretical validation

Length of nanotube	50 nm
Outside Diameter	2 nm
Inside Diameter	1.33 nm
Electrode gap	4 nm
Youngs modulus	1.2 TPa
Electric permittivity (air)	1
Density	2600 kg/m^3

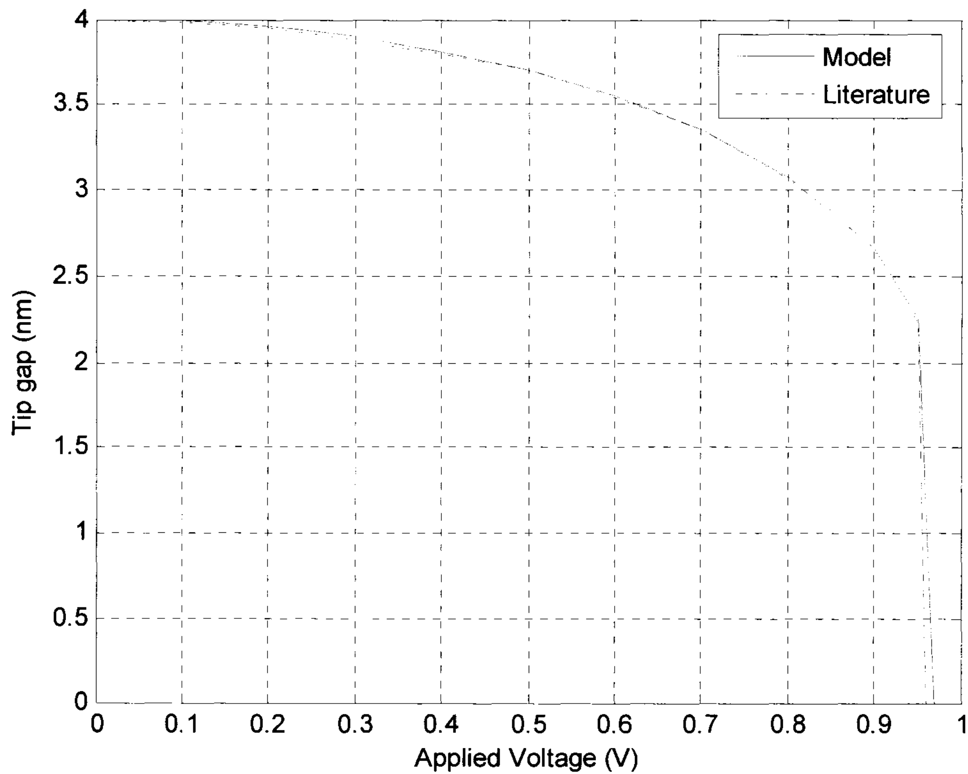

Figure 2.6: Comparison of values of tip gap of the actuator obtained from the theoretical model with the literature [49].

The results above conform very closely to the results in the literature as can be seen from the Figure 2.6.

2.7 SUMMARY

An overview of the modeling and literature of the modeling methods of various electrostatic actuation schemes has been presented. Major influences of the actuators and the perspectives of modeling have been discussed. A unique and generic method of modeling cylindrical electrostatic actuation in both micro and nano domains has been proposed. The method consisted of modeling electrostatic domains and mechanical domains independently using proper assumptions and theories. The capacitance which is the major parameter in the electrostatic force and in the further analysis has been modeled. The coupled electromechanical modeling has been developed using Rayleigh method and the principle of minimum potential energy. A unique iterative approach to solve the nonlinear coupled electromechanical problem has been proposed. Analysis has been performed and important inferences regarding pull in for this special cylindrical actuation have been made. The model has been applied to study the static behaviour of a carbon nanotube actuator. Finally the model has been validated by comparison with the results from the literature. This chapter proposed a method to determine the static behaviour of any cylindrical actuator. But the models cannot capture the interesting dynamic behaviour of the actuators such as switching time and excitation, which is discussed in the following chapter.

CHAPTER 3

DYNAMIC MODELING

3.1 INTRODUCTION

The study of the dynamic behaviour of the mechanical system is one of the key issues in the success of systems in operation. Reliability, efficiency and robustness of the system are important criteria apart from mere functionality defined in static modeling. Dynamic modeling of the system is essential to quantitatively define these important performance criteria before designer can proceed into the optimization and control phase of a design of a product cycle. In MEMS and in specific electrostatic actuators this is very important because of the strong electromechanical coupling involved and possibility of cross talk and cross influences present in the system. Also switching speed is a major criterion for MEMS switches based on electrostatic actuation especially in the applications of radar and wireless communications. Frequency response curves are very important for the resonant mode applications of MEMS devices such as filters, switches and resonators [50]. Many MEMS devices like resonators and accelerometers use external electrostatic forces as a means of tuning the device natural frequency for actively controlling the sensitivity of the device to a broad band of excitation frequencies [51]. Resonant frequency of the MEMS device is an important parameter as it indirectly affects design .Parameters like Q-factor, the switching speed of the device and effects of external noise can all be determined by dynamic study only. A typical electrostatic switch in its closed position bounces several times and then comes into contact to ground electrode. This phenomenon of switch bouncing can drastically reduce the life of a switch and also

the performance. Commonly, in MEMS design, the static pull-in voltage is taken as a criterion. Senturia et al [52] have shown in their simulations that the system may become unstable before this voltage due to the dynamical effect and thus one should consider the dynamic pull-in voltage. This can be seen from the curved path from first equilibrium position to the second unstable equilibrium position shown in the Figure 2.5 of Chapter 2. This is because of dynamic behaviour and this could lead to a dynamic pull in at a very lower applied voltage as opposed to the static pull in which is obtained by just increasing the voltage beyond a point in steady state range. This depends on the amplitude of the resonating actuator and can result in quick failure of the device. Hence to deal with the above problems and get insight into the system dynamic modeling becomes very important.

3.2 EXISTING METHODS OF DYNAMIC ANALYSIS

There are several studies in literature that focus on the dynamic behaviour of the MEMS devices. The major dynamic performance characteristics considered by most of them are [42]:

1. Stability or robustness to parameter variations, structural and environmental changes.
2. Tracking accuracy
3. Disturbance and noise attenuation
4. Transient response parameters, such as, settling time peak time and maximum overshoot.

Different methods have been used in predicting the dynamic behaviour of the system. All of them consider the effect of the electromechanical coupling which is a primordial phenomenon of these actuators. This is very important because the electrostatic forces not only attract the structure to deform but also alter its dynamic properties at the same time. It weakens the structure resulting in elastic softening of the structure. Currently, the established analysis techniques use staggered procedures iterating between the structure on which electrostatic forces are applied and the electrical domain whose boundary follows the structure.

Dynamic behaviour has two parts: steady state response and the transient response. While the steady state response is the response after the actuator has settled and is very important for functionality, transient response is the response to change from equilibrium to other position and is very essential in knowing the time taken for response. The rise time, the over shoot and the settling are all inherent parts of any transient phenomenon. They are used in calculating the switching time of a MEMS device, reliability and life time calculations for fatigue considerations. Also, this is used to study the limiting case of an electrostatic actuator where the overshoot is more than the critical points and could lead to a dynamic pull in. Transient response is very important in RF switches which operate at very high frequency and frequent input excitation results in impulses which may lead to overshoot or relatively higher settling times. Figure 3.1 shows a typical transient curve for an electrostatic actuator. Olivier Francais [53] developed a model and simulator that show the transient response. He used an sinusoidal AC polarization to study the time varying response of the MEMS electrostatic actuator in his work. The effect of various damping factors on the response has been demonstrated

in his work. They also discussed the importance of effect of hysterisis on dynamic pull in and proved that the voltage to pull out the actuator is less than the original value. Stabilization of this transience is a major concern and Joseph et al [54] achieved this by means of a feedback system with an additional series capacitance as shown in Figure 3.1. It can be seen from the transient response curve that the time period for higher voltages is increasing which shows the increase of natural frequency with increasing voltage.

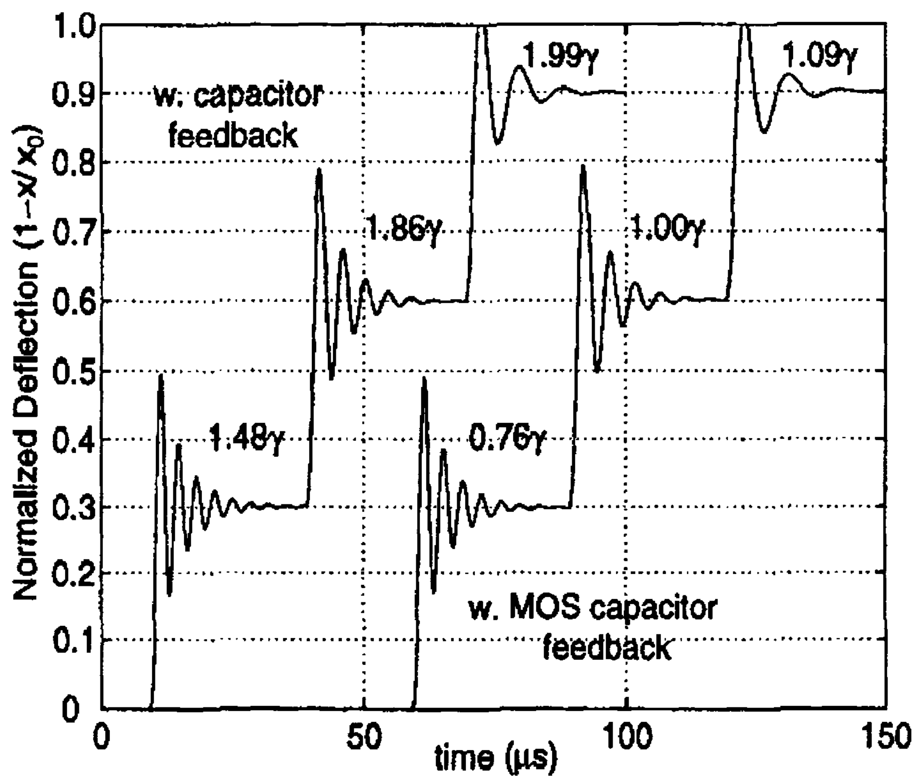

Figure 3.1: Typical transient response curve for an electrostatic actuator [54]

As can be seen from Figure 3.1 damping forces play an important role in determining the dynamic characteristics of a system. In surface micromachined MEMS devices, the major damping mechanism is the squeeze film damping due to viscous dissipation. The

pressure of squeeze film damping has been determined by Chen et al [55] using the simplified form of the Navier–Stokes equation known as the Reynolds equation given by

$$P(x) = \frac{\eta_0 \vartheta}{d_0^3}(L^2 - 4x^2) \tag{3.1}$$

where

As can be seen, this pressure P(x) is a function of the viscosity η_0, electrode gap d_0, length L and velocity ϑ of the structure, and is formulated as an additional force on the system and thus the effect of damping is incorporated in the dynamic model.

Steady state modal analysis is the first step in the analysis and is the scope of this work. This has three stages: Description of the system behaviour and formulating equations of motion and the second step in considering lumped or distributed models of system and finally discretisation using finite element or equivalent techniques. Dynamic analysis is performed either by numerically integrating nonlinear equations of motion, or analytically by linearizing the electrostatic actuation. A wide array of Lagrange methods has been used to formulate the equations of motion using generalized coordinates. Also there exist finite element and boundary element based schemes that perform mechanical analysis on the undeformed geometry of the device using a Lagrangian approach and the electrostatic analysis on the deformed geometry. Such approaches are defined as semi-Lagrangian schemes. It has been reported in [50] that the use of full Lagrange method is far efficient than semi Lagrange method. Boundary elements are also used in order to avoid moving mesh issues. Another approach consists of using predefined capacitance between structural nodes or applying structural reduction techniques together with finite difference evaluation of electrical coupling. Dynamic electrostatic distributed load solver

(*DEDS*) is an another method in the literature to solve the dynamics of electrostatic MEMS, presented in this article. This models the electrostatic force as an equivalent pressure load and also as an embedded stiffness. This is similar to the method of elastic foundation used by Gino et al in [56]. Keeping the cylindrical geometry of the actuators in mind, this thesis formulates a full Lagrange analytical approach in studying the modal behaviour of the system. The variation of the mechanical and electrical forces with respect to small potential and displacement perturbation is an important characteristic of the coupled system as it allows the evaluation of linear vibrations around equilibrium positions and gives an indication of non-linear dynamic and static equilibrium configurations. The tangent stiffness matrix around a reference position is obtained by linearization of the internal forces. The details of the method are presented in the next section.

3.3 DYNAMIC MODELING METHOD USED IN THE THESIS

Figure 3.2. shows the line diagram of a vibrating electrostatic actuator. It can be clearly seen that the mean position of this actuator is not the position at rest and is the static equilibrium position. This position determines the electrostatic force present on the device and thereby the stiffness of the system at any applied voltage. Hence the evaluation of the static deflection Y(x) of the actuator is required to compute the mode shapes. The dotted line represents the general mode shape corresponding to the resonant frequency vibrating with amplitude of $Y^d(x)$.

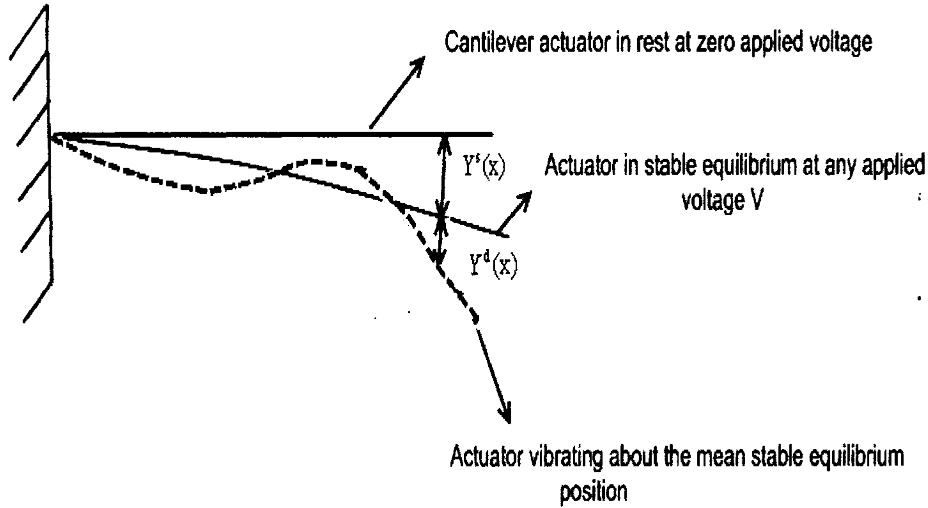

Figure 3.2: Schematic line diagram showing the mode shape of a vibrating cantilever

Rayleigh-Ritz method is used in modeling the dynamic behaviour of the system. It not only provides more accurate values for the fundamental frequency but also gives approximations to the higher natural frequencies and mode shapes. In this method, the vibration deflection shapes are assumed to be in the form of linear combination of polynomial functions which satisfy at least the geometrical boundary conditions of the vibrating structure [57]. The higher the number of polynomials the higher is the accuracy of the natural frequencies obtained. The deflection of the beam due to vibration is given as

$$Y^d(x) = \sum_{i=1}^{n} A^d{}_i \phi^d{}_i(x) \tag{3.2}$$

Where $Y^d(x)$ is the mode shape of the beam with respect to the static position as can be seen from the Figure 3.2, the $A^d{}_i$ are the deflection coefficients and the $\phi^d{}_i$ are the orthogonal polynomials generated by Gram-Schmidt orthogonolization procedure. x is a

non dimensionalised position variable which varies from x=0 at fixed end to x=1 at the free end. The squeeze film damping and its effects have been neglected as the deflection and thereby the displacements of the particles are very small relative to the size of the cantilever waveguide. This method assumes a harmonic motion in free vibration which means that the vibrating displacement which is a function of space and time as Y =f(x, t) can be separated in time and space given by the equation,

$$Y = Y^{d}(x) * \sin(\omega t) \tag{3.3}$$

This uses the principle that maximum kinetic energy is equal to the maximum potential energy,

$$U_{max} = T_{max} \tag{3.4}$$

(OR)

$$\omega^2 = \frac{U_{max}}{T^{*}_{max}} \tag{3.5}$$

Where $T_{max} = \omega^2 T^{*}_{max}$ and ω^2 is known as Rayleigh's quotient.

The kinetic energy of the non-dimensionalised beam is given by,

$$T = \frac{1}{2} L \int_0^1 mv^2 dx \tag{3.6}$$

The maximum kinetic energy of the beam is given as,

$$T_{max} = \frac{1}{2} m \int_0^1 L(Y(x))^2 \omega^2 dx \tag{3.7}$$

Where

m- mass of the beam per unit length

L- Length of the beam

ω - Natural frequency

The maximum potential energy of the beam is given by

$$U_{max} = U_{BEAM} + U_{ES} \tag{3.8}$$

Where U_{ES} and U_{BEAM} are the same expressions obtained from Chapter 2 in which the Y(x) is replaced by $Y_d(x)$. The maximum potential and kinetic energies are formulated using the assumed deflection shapes from Equation (3.2) and are used to obtain an expression for the natural frequency in the form of Rayleigh quotient.

$$\omega^2 = \frac{U_{max}(A_1^d, A_2^d, A_3^d....)}{T^*_{MAX}(A_1^d, A_2^d, A_3^d....)} \tag{3.9}$$

At this point the coefficients A_i^d (i = 1 to n) are adjusted so that the frequency is made stationary at the natural frequency with respect to each coefficient, (i.e)

$$\frac{\partial \omega^2}{\partial A_i^d} = 0 \tag{3.10}$$

This results in a linear system of 'n' number of equations that forms the Eigenvalue problem,

$$\sum_n [K_{beam}^{i,n} - K_{ES}^{i,n} - \omega^2 M^{i,n}] A_n^d = 0 \tag{3.11}$$

Where the following definitions apply,

$$K_{beam}^{i,n} = \frac{EI}{L^3}\int_0^1 (\frac{d^2\phi_n^d(x)}{dx^2})(\frac{d^2\phi_i^d(x)}{dx^2})dx \tag{3.12}$$

$$K_{ES}^{i,n} = L\int_0^1 K_{ES}(x)\phi_n^d(x)\phi_i^d(x)dx \tag{3.13}$$

$$M^{i,n} = mL\int_0^1 \phi_n^d(x)\phi_i^d(x)dx \tag{3.14}$$

Where,

$K_{beam}^{i,n}$ is the stiffness matrix of the beam

$K_{ES}^{i,n}$ is the electrostatic spring stiffness matrix

$M^{i,n}$ is the mass matrix from the inertial components of the moving structure.

Solving Equation (3.11) leads to natural frequencies and mode shapes of the system. The functions $\phi_i^d(x)$ assumed in this section to describe the mode shape are algebraic functions and polynomials of higher degree. They are carefully selected to describe the boundary supports and the constraints of the cantilever and are discussed in the following section.

3.3.1 BOUNDARY CHARACTERISTIC ORTHOGONAL POLYNOMIALS

Boundary characteristic orthogonal polynomials are polynomials that are used to describe the deflection shape in static analysis and the mode shape of the structure in dynamic analysis. As the name indicates they try to represent the boundary conditions of the structure. They also form an orthogonal set of polynomials and they are generated by

popular Gram-Schmidt orthogonolization process [58] as given by the following formulation,

$$\phi_1(x) = (x - B_1)\phi_0(x) \tag{3.15}$$

$$\phi_k(x) = (x - B_k)\phi_{k-1}(x) - C_k\phi_{k-2}(x) \tag{3.16}$$

$$B_K = \frac{\int_a^b xw(x)\phi_{k-1}^2(x)dx}{\int_a^b w(x)\phi_{k-1}^2(x)dx} \tag{3.17}$$

$$C_k = \frac{\int_a^b xw(x)\phi_{k-1}(x)\phi_{k-2}(x)dx}{\int_a^b w(x)\phi_{k-2}^2(x)dx} \tag{3.18}$$

The polynomials generated by this method satisfy the condition

$$\int_a^b w(x)\phi_k\phi_{m \neq k}(x)dx = 0 \tag{3.19}$$

The main advantage of this orthogonolization process is in the computation of the stiffness matrix and the mass matrix of the system in an eigenvalue problem where all the non diagonal elements become zero and eliminates the possibility of generation of ill conditioned matrices in the final result.

The weight function in this case is taken as 1. The range a to b is 0 to 1 as the non dimensionalised variable x varies from 0 to 1 which represents the length of the cantilever. The first polynomial is chosen to satisfy all the essential and natural boundary conditions of the cantilever beam fixed at one end and free at the other end. The essential or the geometrical boundary conditions that describe a cantilever fixed at one end are

1) Deflection at the fixed end is zero given by,

$$\phi_1^d(0) = 0 \tag{3.20}$$

2) The slope at the fixed end is zero given by,

$$\left.\frac{d\phi_1^d(x)}{dx}\right|_{x=0} = 0 \tag{3.21}$$

The natural boundary conditions that describe the freely vibrating cantilever without a time varying external force are

1) The moment at the free end is zero given by

$$\left.\frac{d^2\phi_1^d(x)}{dx^2}\right|_{x=1} = 0 \tag{3.22}$$

2) The shear at the free end is zero given by

$$\left.\frac{d^3\phi_1^d(x)}{dx^3}\right|_{x=1} = 0 \tag{3.23}$$

Assuming the polynomial as an algebraic function of the form

$$\phi(x) = a_0 + a_1 x + a_2 x^2 + a_3 x^3 + a_4 x^4 \tag{3.24}$$

And substituting the expression in all the boundary conditions give the shape as

$$\phi_1^d(x) = x^4 - 4x^3 + 6x^2 \tag{3.25}$$

This is chosen as the first polynomial. The higher polynomials are generated by the Equations (3.15) – (3.18). The number of polynomials chosen in the computation depends upon the required number of the higher frequencies and mode shapes and also on

the desired accuracy of the natural frequencies [59]. In this case first and second natural frequencies are of importance and hence two polynomials are used for the computation.

3.3.2 ELASTIC FOUNDATION

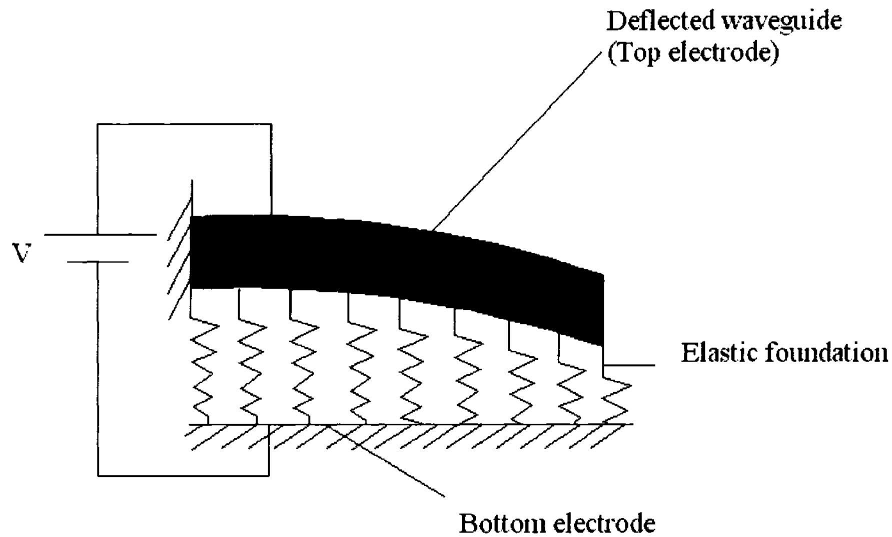

Figure 3.3: Elastic foundation representation of the electrostatically actuated waveguide.

Clearly the capacitance from Equation (2.4) indicates the nonlinear nature of the electrostatic force. This makes it difficult to solve for dynamic analysis as it would not lead to a standard eigenvalue problem in Equation (3.11). Hence to linearise the electrostatic energy, an equivalent model of the beam using an elastic foundation is considered for further analysis as shown in Figure 3.3. Boundary conditioning is a way of modeling the influence of structural, support and environmental operating conditions on the elastic property of the system using artificial springs [56]. In this case, the external force or the electrostatic force is modeled as a boundary with the same effect. The influence is represented by an elastic foundation which consists of a series of discrete

springs. These springs are negative in their operation as they soften the system instead of stiffening the system.

The electrostatic force is replaced by linear springs of varying stiffness $K_{ES}(x)$ along the length of the beam as given in Equation (3.27). As the cantilever vibrates in small amplitude about the static equilibrium position, the stiffness can be evaluated as the rate of change of the electrostatic force about this equilibrium position. This assumption is very good for small amplitudes of vibrations. The stiffness is evaluated at the static equilibrium position as the slope of the tangent at the point of intersection of the electrostatic curve and the mechanical linear force line as seen in the following Figure 3.4.

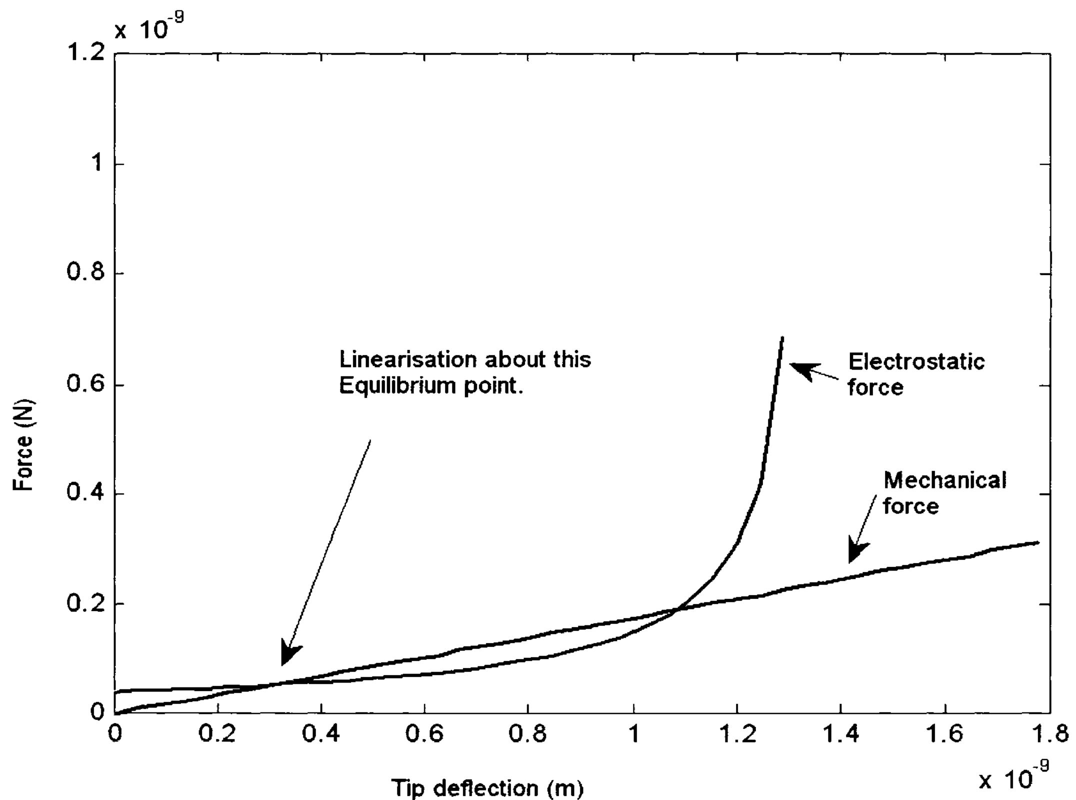

Figure 3.4: Typical force balance curve showing the point of linearization for small amplitude of vibrations

The electrostatic force at the static equilibrium is given by,

$$F_{ES} = \frac{dUelec}{dA_i} = \int_0^1 \frac{\pi\varepsilon_0\varepsilon_r V^2 \phi_i L}{R\sqrt{\frac{r(x)(r(x)+2R)}{R^2}}\log^2\left[1+\frac{r(x)}{R}+\sqrt{\frac{r(x)(r(x)+2R)}{R^2}}\right]} dx \qquad (3.26)$$

and the Stiffness of the elastic foundation per unit length is given by,

$$K_{ES} = \frac{dF_{ES}}{dA_i} = \frac{\pi\varepsilon_0\varepsilon_r V^2}{R^2 P^3 \log^3[Q+P]}[Q\log[Q+P]+2P] \qquad (3.27)$$

Where the following definitions apply,

$$P = \sqrt{\frac{r(x)(r(x)+2R)}{R^2}} \qquad (3.28)$$

$$Q = 1+\frac{r}{R} \qquad (3.29)$$

The variation of this equivalent stiffness along the length of the beam has been plotted for a voltage of 10 volts and electrode gap of 60 microns and 10 mm length waveguide in Figure 3.5. This shows the non uniform variation of the electrostatic force along the length of the beam. Then electrostatic energy is estimated as

$$U_{ELEC} = \frac{1}{2}L\int_0^1 K_{ES} Y_d^{\,2} dx \qquad (3.30)$$

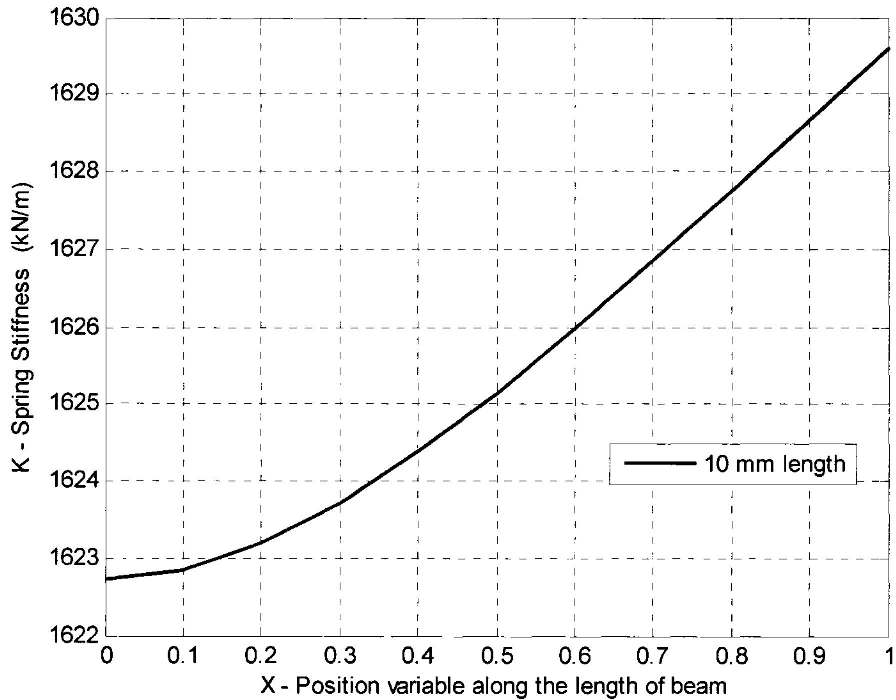

Figure 3.5: Variation of K_{ES} for an applied voltage of 10V and an electrode gap of 60 microns.

3.4 VALIDATION OF THE MODEL

The mathematical model as mentioned in the earlier chapters can be very well applied to nano actuators of cylindrical shape. In this section, the model is used to study the dynamic behaviour of a carbon nano tube resonator. The results obtained from our model are compared with results from the literature [60]. Philippe Poncharal et al [60] did work on the electro mechanical resonances of carbon nanotubes and found the first two natural frequencies of these nanotube resonators as given in Table 3.1. The Figure 3.6 shows the actuator vibrating at static position and in first and second mode shapes, respectively. The Table 3.2 gives the list of parameters that describes the configuration of the device used in the validation of the model including the dimensions of the

nanotubes and the electrode gaps used. The results are tabulated in Table 3.1. It can be seen that the present model obtained a first natural frequency of 473 kHz compared to 530 KHz from the literature. This is very close for nano scale and this validates the present model.

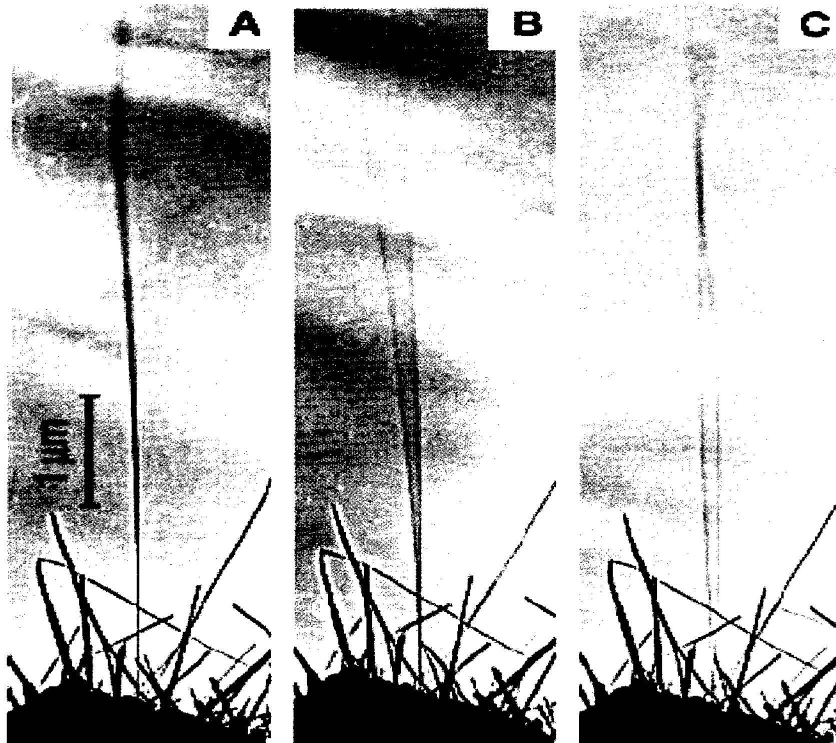

Figure 3.6: Mode shapes of carbon nano resonators A) at no voltage and noise, B) First mode, C) second mode [60]

Table 3.1: Comparison of the model results of natural frequencies with values from literature [60]

	First natural frequency	Second natural frequency
Our model	473 kHz	3.502 MHz
Literature	530 kHz	3.01 MHz

Table 3.2: List of parameters used in the validation of the model.

Diameter of the carbon nanotube	14.5 nm
Length of the carbon nanotube	6.25 μm
Youngs modulus	0.21 TPa
Electrode gap	10 μm
Density	2600 kg/m^3
Electric permittivity of air	1.0

3.5 SUMMARY

The importance of dynamic analysis of MEMS devices in their design is discussed. Existing methods of modeling the transient and steady behaviour of the MEMS devices have been presented. A full Lagrange method of Dynamic modeling has been presented using Rayleigh Ritz energy method. A method of generating orthogonal polynomials using Gram Schmidt orthogonolization procedure is used to well condition the matrices of the eigenvalue problem. A unique method of boundary conditioning using artificial springs to represent the external electrostatic forces as inherent negative stiffness of the system is presented and thereby linearising the problem. The dynamic model has been used to study the dynamic behaviour of a carbon nanotube resonator and is validated by comparing with results from the literature. Also the presence of modal stiffness in the system has been observed due to inherent residual stresses and curvatures in the structure which is noticed from the variation in the trend of the comparison between the results for the first and second natural frequencies .

CHAPTER 4

DESIGN OF A VARIABLE OPTICAL ATTENUATOR

4.1 INTRODUCTION TO VOA DESIGN

A brief introduction on optical attenuation and literature review of attenuators has been presented in the Chapter 1.4 . The rationale of choosing waveguide attenuation scheme and a novel fiber based VOA has also been presented. This chapter presents the proposed design scheme in detail and describes the design of VOAs. Design in general is an iterative phenomenon in evaluating the best and optimum trade-off between performance, cost and manufacturing feasibility or manufacturability. The present thesis concentrates on design for performance. Figure 4.1 shows a typical MEMS design chart [61]. As can be seen from the figure, the design of MEMS device is mainly influenced by the transduction method and the fabrication methodology. Also it is a trade-off between functional and performance requirements, and capabilities of the technology. Hence this chapter starts by explaining the proposed scheme and the transduction methods and then fabrication constraints of the scheme. Modeling of the system is established and then the set of model parameters that act as input for the design are also identified. Then, the parametric analysis is performed to study the performance characterization of the device against these model parameters. Also the functional requirements of a typical VOA are discussed and used to design the VOA. The capabilities and details of the scheme and the detailed design procedure are presented in the following subsections.

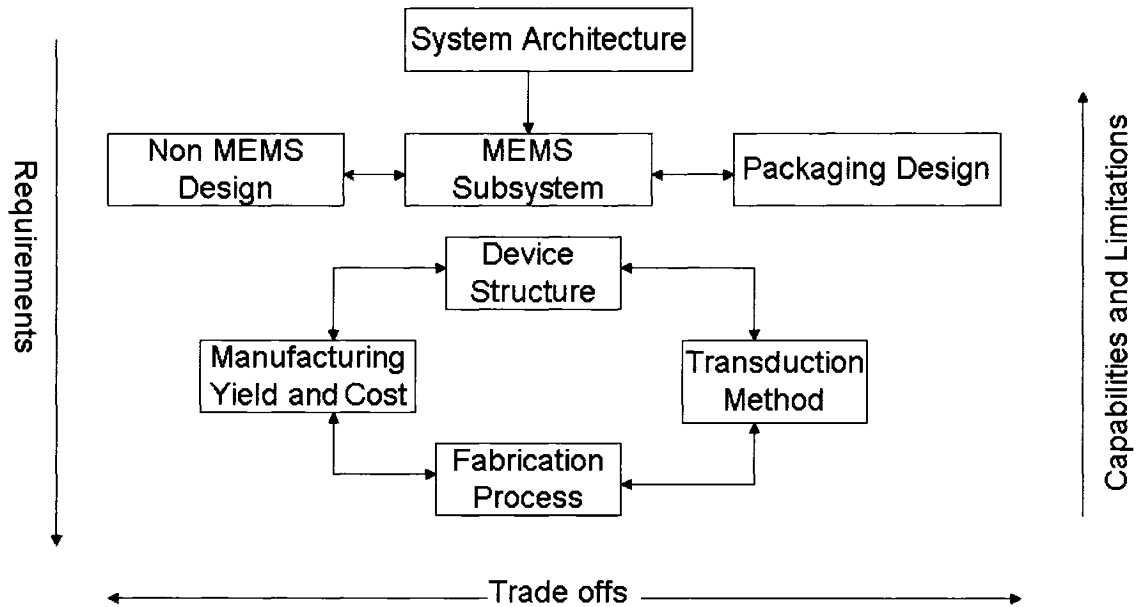

Figure 4.1: Typical MEMS Design Methodology

4.2 PROPOSED VOA DESIGN

The schematic illustration of the proposed device design is shown in Figure 4.2. Any design is not complete without fabrication and it makes no meaning without the feasibility of fabrication. Hence, the possible fabrication methodology is also discussed along with the topography and principle of the device. The device comprises of an input fiber and output fiber inserted in V-grooves. The input fiber is allowed to overhang at the end by completely removing portion of the silicon substrate. The V-grooves and the electrode gap are etched out of a silicon substrate using bulk micromachining. The overhanging length of fiber is coated with metal, thereby making it a movable electrode. The bottom of the substrate, acting as bottom electrode plate, is also coated with metal. A bias Voltage applied between the two electrodes creates charge distribution on the surfaces of the electrodes creating an electrostatic force. This force actuates the movable electrode and creates a lateral mismatch, equal to the tip deflection, with the output fiber,

generating attenuation to the signal. There is also certain amount of angular misalignment at the end of the fiber because of slope of the tip of the deflected waveguide and this would add to the total attenuation of the device. This device is tunable or it is a variable optical attenuator as the attenuation levels can be continuously varied using the applied voltages and this makes it an ideal application for equalizers. A continuous array of these V grooves can be fabricated on this device and could be used to equalize different channels of multiplexers in WDM networks.

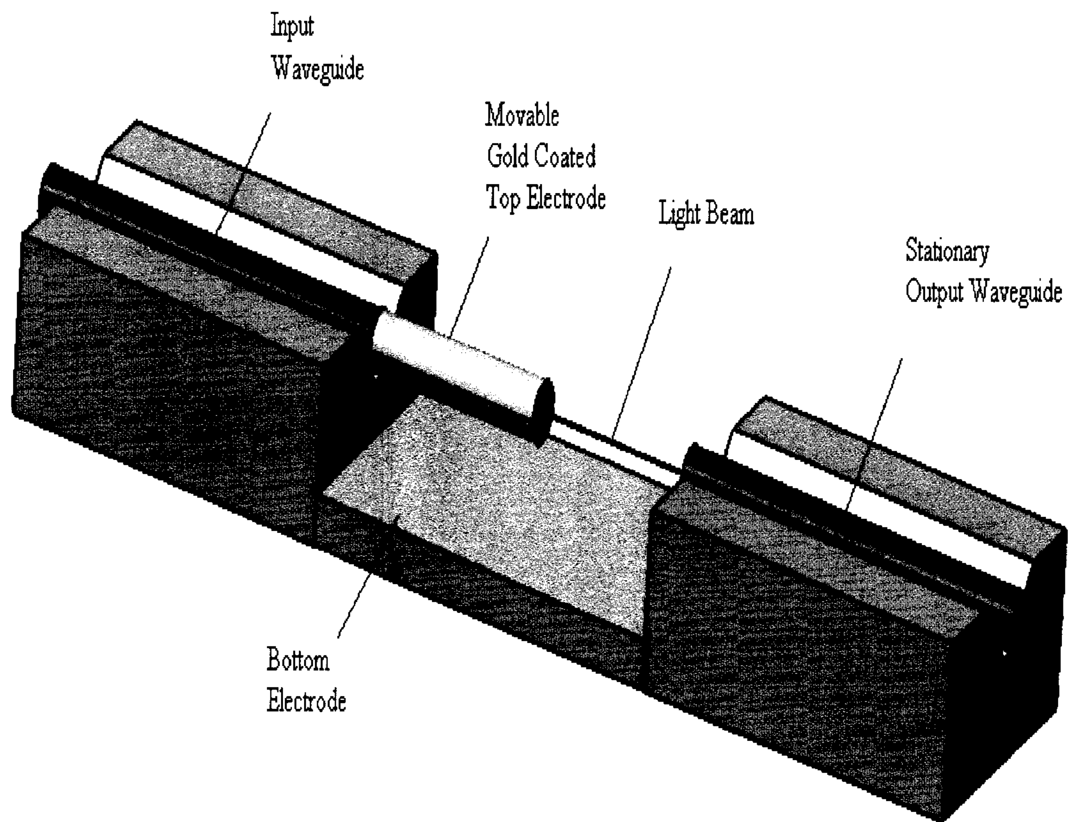

Figure 4.2: Schematic of the electrostatically actuated cylindrical waveguide based variable optical attenuator

4.3 OPTICAL MODELING

As described in the previous section, the proposed scheme utilizes electrostatic actuation of a cylindrical waveguide for the attenuation. Hence, the generic electromechanical modeling of cylindrical actuation proposed in the previous chapters can be employed for the static and dynamic analysis of the system. But the optical modeling that relates the actuation and the corresponding misalignments of the input waveguide to the amount of light coupled into the output waveguide is presented in this section. Gaussian beam theory has been used for modeling the propagation of the light beam in the free space between the two waveguides.

The following assumptions have been used throughout the model.

- The fibers used in the modeling are single mode fibers with clad diameter equal to 125 microns
- The light beam that emerges out of the optical fiber waveguide is a Gaussian beam
- The waist diameter w_0 of the gaussian beam is approximately equal to that of the core diameter.
- The input and the output fibers are assumed to be apart at a distance of 30 μm so that the loss due to mode mismatch and separation of the fibers can be neglected.

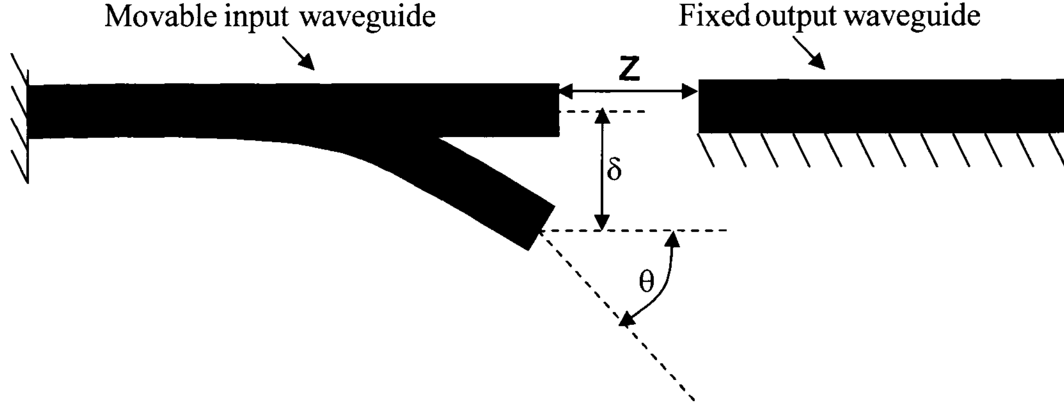

Figure 4.3: Exaggerated Schematic showing attenuating fiber due to lateral and angular misalignment

According to this theory, the coupling efficiency due to both lateral and angular mismatch has been evaluated using the following equations [62, 63],

$$\eta_{lateral} = e^{-\left(\frac{\delta}{w_0}\right)^2} \tag{4.1}$$

$$\eta_{angular} = e^{-T^2} \tag{4.2}$$

$$T = \frac{\sin\theta}{\frac{\lambda}{n_0 \pi w_0}} \tag{4.3}$$

where δ is the lateral mismatch, θ is the angular misalignment between the fibers which is equal to the slope of the cantilever at the tip, λ is the free space wavelength

equal to 1.55 μm, n_0 is the refractive index of the medium equal to one for air and w_0 is the waist radius of the beam at the plane of the output fiber. Figure 4.3 clearly describes the terms used in the modeling and the attenuation principle.

The total coupling efficiency for the beam is evaluated by

$$\eta_{total} = \eta_{lateral} * \eta_{angular} \tag{4.4}$$

The insertion loss in dB is obtained using the formula

$$\text{loss}(\text{dB}) = -10\log_{10}(\eta_{total}) \tag{4.5}$$

4.4 DESIGN CRITERION

As already discussed in the Chapter 1.4, the main aim of attenuation schemes is to have controllable device attenuation in a continuous range to match with the dynamic range of the receiver. All other uncontrollable losses have to be minimized which include polarization dependent loss (PDL), reflection loss (RL) and wavelength dependent loss (WDL). This proposed attenuation scheme takes care of these requirements by minimizing these losses. Also from viewing the commercial market and literature, the major requirements for VOA are continuous range of attenuation up to 50 dB and a driving voltage within 50 Volts. As the design criteria have been defined, the next step would be to identify the variable parameters of the method which include geometric and process parameters. Since the process parameters depend upon the micro fabrication, the key parameters that affect the design are the applied voltage, the length of the fiber waveguide, the electrode gap and then the separation between the input and output waveguides.

4.5 PARAMETRIC STUDY

Considering the above defined design requirements and capabilities of the scheme, parametric analysis is carried to characterize the performance of the design by varying the design parameters. Coupling efficiencies and thereby insertion losses for selected fiber lengths of 10mm, 15mm and 20 mm have been evaluated using the optical model of Section 4.3 for selected electrode gaps of 30 and 60 microns. Tip deflections have been evaluated using the mechanical models in 2.5. The results are shown in Figures Figure 4.4 to Figure 4.9. Clearly, fibers of higher lengths and lower gaps give higher attenuation. But, every electrostatic actuator has an inherent property called pull-in voltage where it snaps down. Higher lengths have lower snap voltages as seen for 15 mm and 20 mm fibers in Figure 4.5. Also only a portion of the total electrode gap can be used for the range of travel of the actuator as it is limited by the pull-in. This limit of actuation is the same for any fiber independent of the lengths as can be seen from tip deflections of the 15 mm and 20 mm fibers in Figure 4.5 at their pull-in voltages of 26 and 46 volts respectively. Both have the same maximum tip deflection of 14 microns for an electrode gap of 30 microns. Figure 4.6 and Figure 4.7 show the variation of coupling efficiency while Figure 4.8 and Figure 4.9 represent the insertion losses for different geometrical configuration against the applied voltage. At higher voltages, small change in voltage causes a higher attenuation change and hence controllable actuation can be achieved only well before the pull-in voltage. From Figure 4.9, attenuation over 30 dB has been obtained for fiber lengths of 20 and 15 mm, respectively, for the selected voltage range.

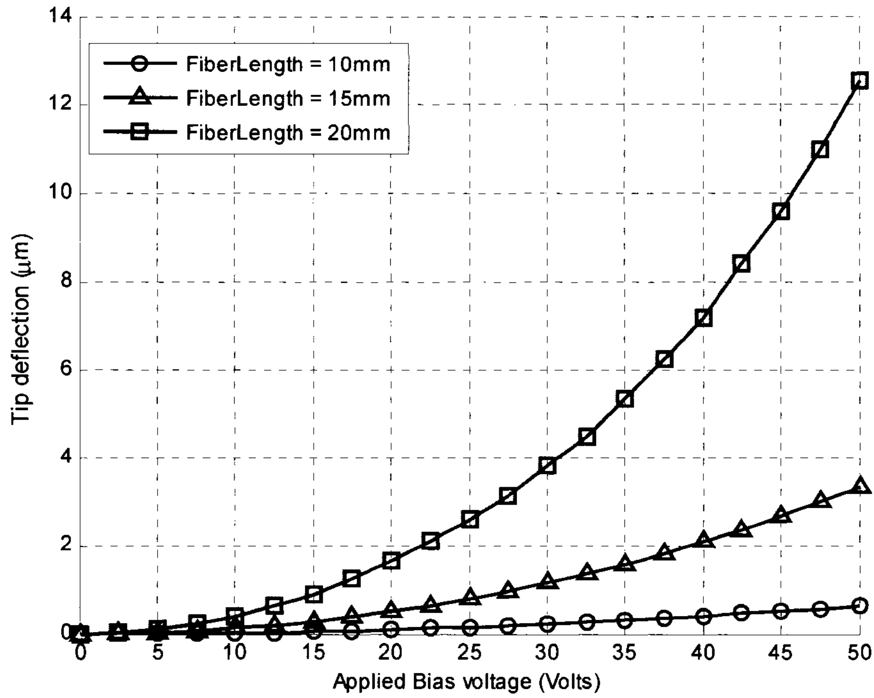

Figure 4.4: Tip deflection of waveguide for an electrode gap of 60 microns for various voltages

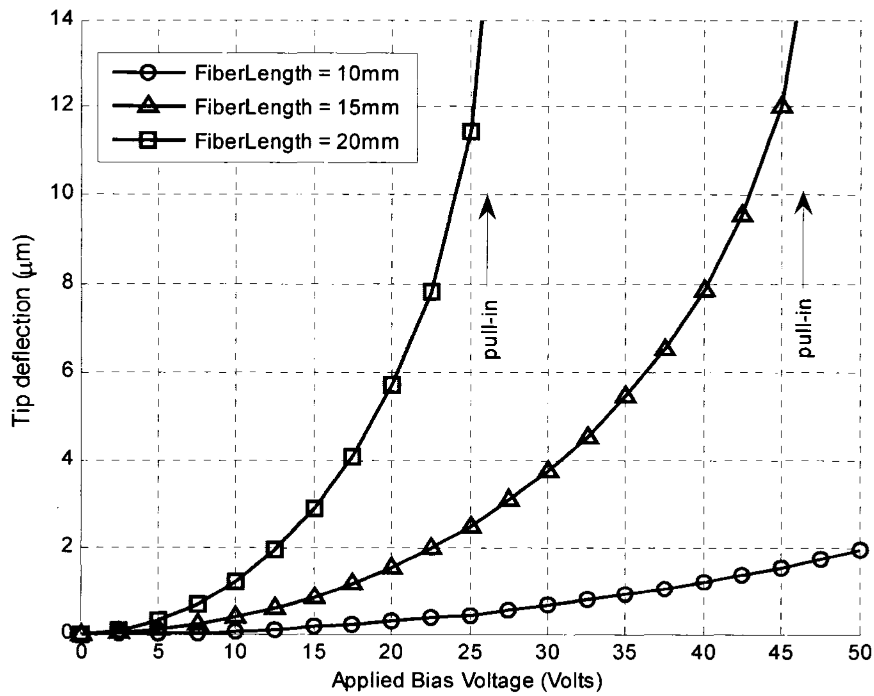

Figure 4.5: Tip deflection of waveguide for an electrode gap of 30 microns for various voltages

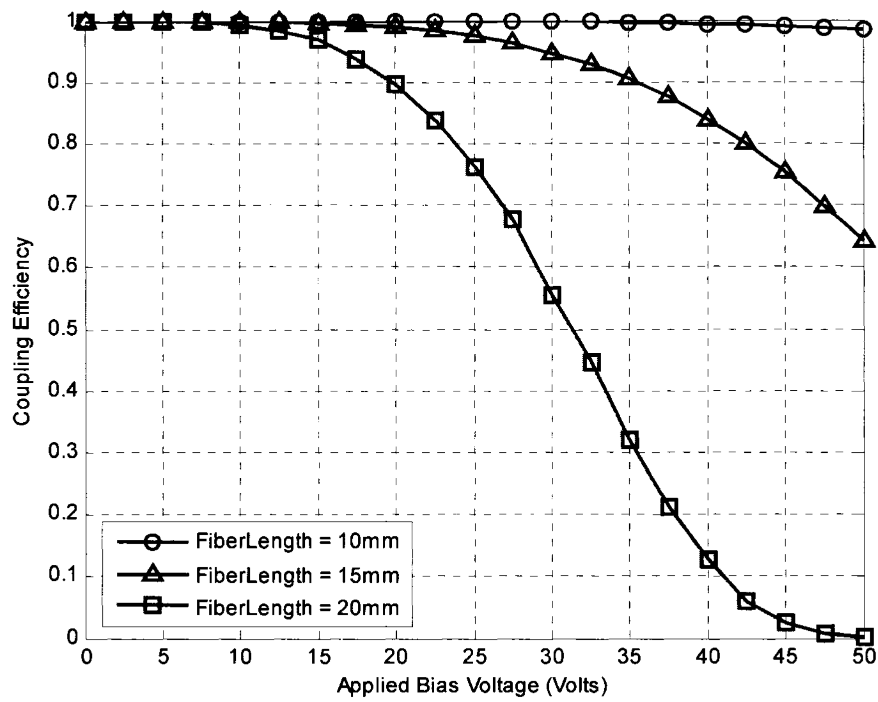

Figure 4.6: Coupling efficiency of waveguide for an electrode gap of 60 microns for various voltages

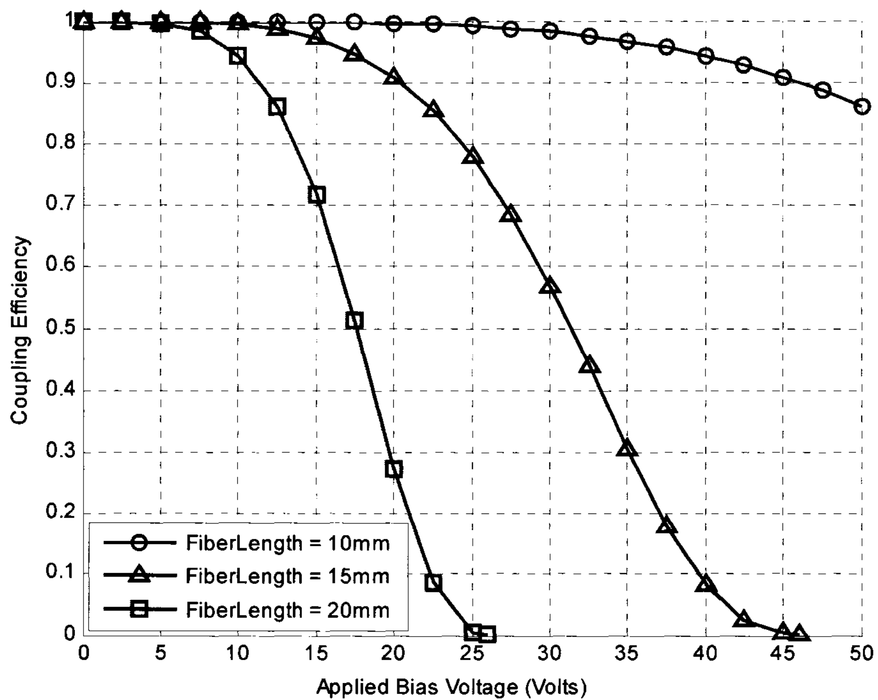

Figure 4.7: Coupling efficiency of waveguide for an electrode gap of 30 microns for various voltages

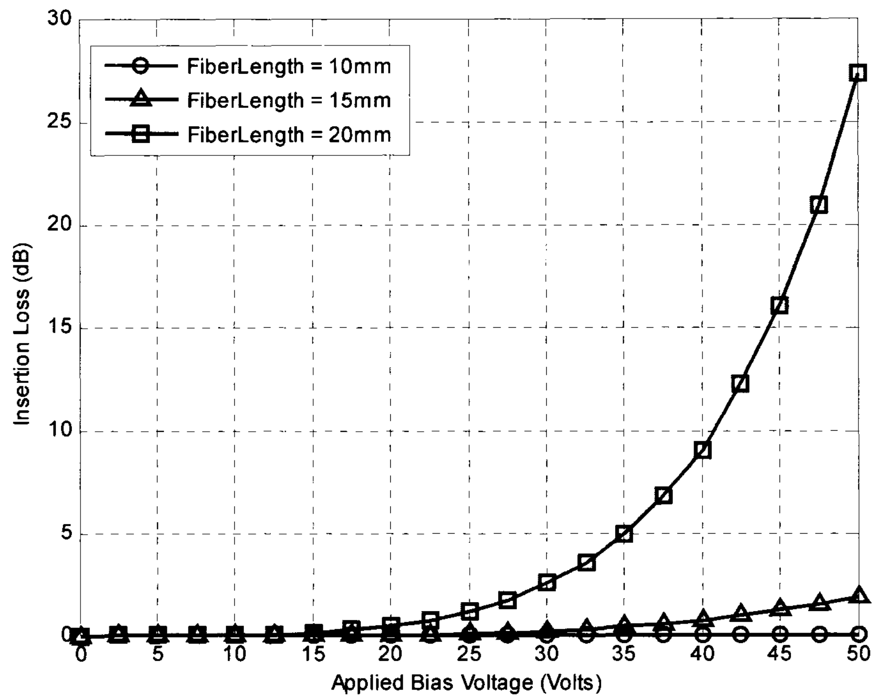

Figure 4.8: Insertion loss/attenuation for an electrode gap of 60 microns for various voltages

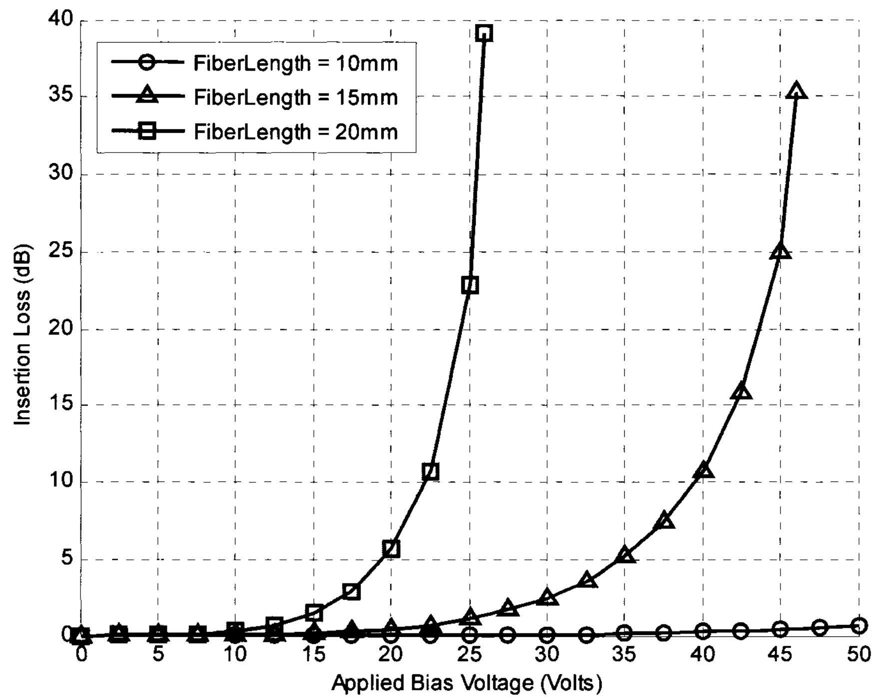

Figure 4.9: Insertion loss or attenuation for an electrode gap of 30 microns for various voltages

4.6 DYNAMIC ANALYSIS

The natural frequencies of the waveguides have been evaluated using the model in Section 3 by varying these key parameters to study their influence on the stability of the system. Fiber lengths of 10mm, 15mm and 20 mm and electrode gaps of 30 and 60 microns have been considered for evaluating the model. The results are shown in Figures 4.10 and 4.11. It can be clearly observed that the natural frequencies decrease with increasing voltage. This is due to the negative stiffness of the electrostatic force. This clearly demonstrates the spring softening effect of the electrostatic force which causes a decrease in the total stiffness of the system and thereby leading to lower natural frequencies. Also, it can be observed that the 10 mm and 15 mm length fibers have a zero natural frequency at voltages of 25 and 43 volts. These voltages correspond to the snap point where the actuator touches the bottom of the electrode. It can be observed that the natural frequencies increase with decreasing length. Also, as the electrode gap decreases the natural frequencies in figure 4.11 decreases at a higher rate compared to Figure 4.10 and hence snap voltages are lower for low electrode gaps. The exponential nature of the electrostatic force can also be observed from these graphs.

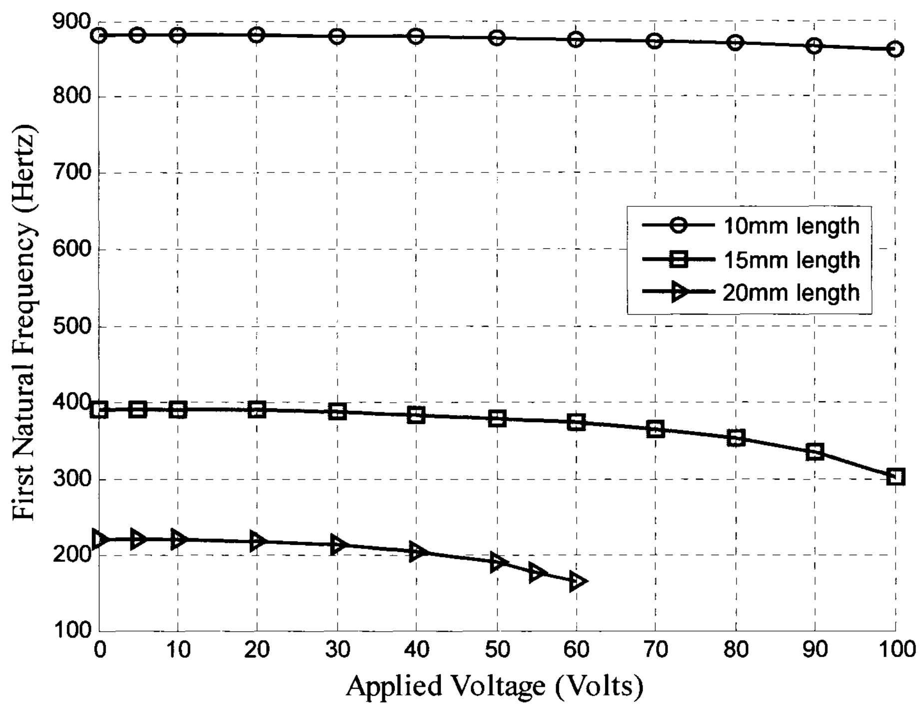

Figure 4.10: Natural frequency Vs voltage for various lengths of waveguides at an electrode gap of 60 microns

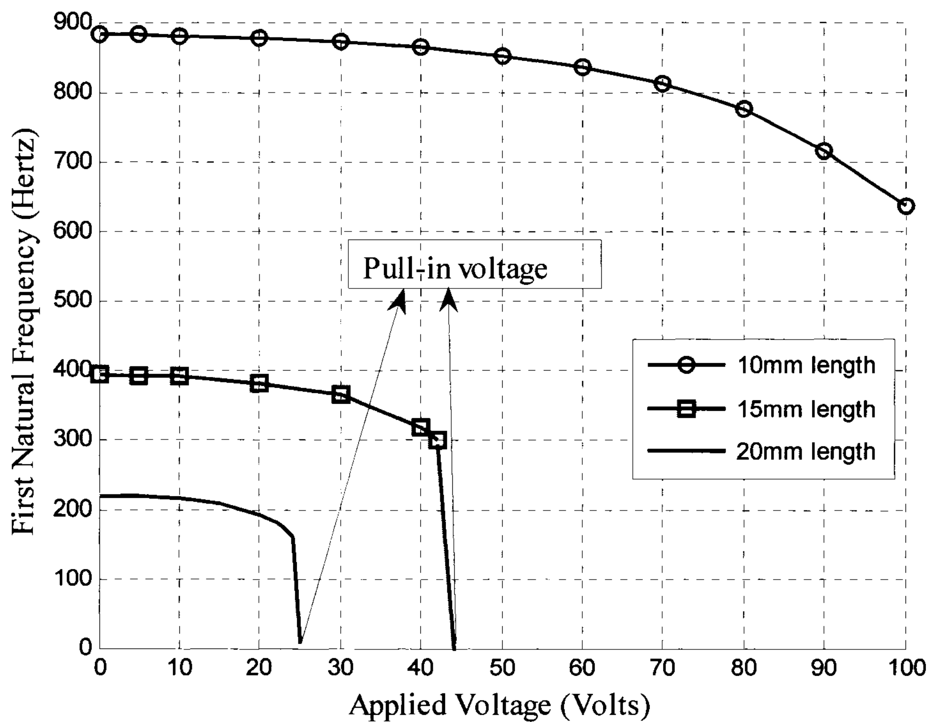

Figure 4.11: Natural frequency Vs voltage for various lengths of waveguides and electrode gap of 30 microns

4.7 SUMMARY

This chapter has introduced the design methodologies of VOA devices. It also introduced a novel method of optical attenuation using direct actuation of a waveguide. The capabilities and limitations of the model have been discussed in par with the requirements of the industry. Important design parameters have been identified and have been used in parametric characterization. Finally designs showed a continuous range of attenuation from 0 to 25 dB with voltages less than 50 volts. This shows the possibility and feasibility of the proposed method. Also dynamic analysis of the VOAs has been presented. The softening of the structures due to the negative stiffness of the electrostatic force was observed. The pull-in voltages of the electrostatically actuated waveguides have been predicted by the model. The results from the model can be used in the process of the VOA to avoid resonance and snap down of the structures which are critical properties that limit the functionality of the VOA. The knowledge of the resonant frequencies could be used to tune them for varying the switching speed of these VOAs. The next phase of this design would be experimental testing of the designed device which is discussed in Chapter 5.

CHAPTER 5

EXPERIMENTAL ELECTROMECHANICAL TESTING AND VALIDATION

5.1 INTRODUCTION

In Chapters 3 and 4, modeling and analysis of the system has been described for understanding the static and dynamic behaviour of cylindrical actuator. The models were based on certain assumptions and simplifications in predicting the behaviour of the system. In order to know how accurately these models represent the real system, experimental testing and validation of the results obtained from the testing is mandatory. In this chapter, experimental testing of the system including the test setup, testing procedure and test results are discussed. Microfabrication and the constraints in the process can vary the real system from the ideal hypothesized system in many ways. Residual stresses and surface roughness are few of the major processing related properties that can affect MEMS devices. Also, theoretically classical and ideal conditions may not prevail like the presence of non ideal boundaries and supports in final fabricated devices. Hence, testing becomes an important part of the product development process and in moving the devices from lab to fab. The smaller dimensions involved in MEMS poses a great challenge in testing these devices. Different techniques exist that are used to test micro devices and characterize their behaviour to various external stimuli. An introduction to these methods and their advantages and disadvantages are presented in this following section.

5.2 EXISTING TESTING TECHNIQUES

MEMS testing comprises of Functional testing, reliability testing and failure testing of the device and its packaging. Reliability testing is a measure of the longevity and consistency of operating device and it involves measurement over a long period of time. This is often environmental and involves testing system for various external factors, such as, temperature, humidity, external disturbances, etc. [64]. Failure testing and fatigue characterization including crack initiation, propagation, failure modes are also very important for long life of designed MEMS. Material characterization is also a major area of experimental testing as many modern applications of MEMS started using non-silicon materials whose mechanical properties and optical properties are still being explored. Especially polymers like PVDF (PolyvinylideneDiflouride) and PDMS (Polydimethylsiloxane) have attracted many researchers.

Functional testing involves static and dynamic testing. Both generally involve three components: visualization, measurement of actuation and motion detection. Both two dimensional and three dimensional visualization tools exist and they are used to describe the topography of the MEMS devices. Typical experimental tools for 3d visualization of MEMS or its topography include AFM cantilevers, optical profilers, and stylus profilers [65]. Measurement of the actuation is done by sensing elements that are further connected to a control loop mechanism to give feedback to the source of actuations about the accuracy in required input. Motion detection involves both in-plane deflections as in comb drive actuators and out-of-plane deflections as in parallel plate actuation mechanisms.

Out of plane motion is the vertical motion that is usually critical to device operation and hence, accurate measurement of these small movements is essential to characterize device behavior. A wide variety of techniques, such as, capacitive sensing [66-68], piezoresistive sensing [69] and optical detection [70-72] have been used to measure the out of plane deflection in MEMS structures. Piezoresistive techniques can be used to measure indirectly the deflection of micromachined structures [73]. Piezoresistors are strain gauges that change resistance with a change in dimension. This property is used to detect deflection of the structures. This method is a contact method and can also change the properties of the structures to some extent. Also pull-in phenomenon has been widely used for characterization. Though good at sensitivity, microfabricated capacitive sensors require on-chip electronics due to the small capacitance changes involved [67]. Therefore researchers have been interested in methods that are non-intrusive and that do not require any modifications to the device itself which led to development of optical deflection detection methods. All these optical methods utilize the change in property of the light signal, such as, its physical position, phase shift or intensity variation. A nice example of the former is of an electrostatic actuator driven MEMS device designed by Borovic [74] that utilizes optical modulation to sense displacement. The principle involves two comb drives that move a shutter to modulate a light beam between laser and photo detector. The output voltage from the photo detector was then used to determine the displacement of the shutter assembly. Test setup for static testing vary from direct visual inspections schemes using microscopy, SEM (Scanning electron microscopy) and TEM (Transmission Electron Microscopy) to intereferometric techniques and optical methods using simple reflection of laser beam to

detect the motion [75, 76] . The large field of view and ability to characterize the surface roughness in nanoscopic range and its higher accuracy in measuring the out of plane deflections makes white light interferometry the preferred method in static and dynamic characterization of MEMS. Various principles of interferometry, such as, Phase-Shifting Interferometry (PSI), Vertical Scanning Interferometry (VSI) and High-Definition Vertical Scanning Interferometry (HDVSI) [65] have been used. A variety of custom systems have been developed relying on interferometry [77, 78]. All these methods generate dark and bright fringes in succession and the processing of these fringes, their geometry and distances between them would directly reveal the deformation profile of the structure.

Dynamic testing, in particular, experimental modal analysis involves measurement of relative surface velocity and thereby the natural frequencies and the corresponding mode shapes. Fewer techniques exist for detecting relative velocity in MEMS devices than for detecting relative displacement. Modal data describes the dynamic properties of a structure and can assist in the design of almost any structure, helping to identify areas where design changes are most needed. LDV (Laser Doppler Velocimetry) and interferometry are again the major methods utilized in this testing. Hence after review of all the testing methods and considering the available systems in the lab, a simple testing method using microscope with an attached ocular micrometer has been used to study the static testing and an LDV based dynamic testing to study the dynamic behaviour. The testing methodology and the results are discussed in the following sections.

5.3 STATIC TESTING

Testing procedure consists of three steps: Setting up the testing scheme, preparing the device and then measurement using instrumentation for an applied voltage. In static testing, the measurement is the deflection of the actuator or its relative position. A simple and efficient direct optical microscopic method is used in finding the deflection of the actuator. This method could be used to measure the deflection all along the length of the beam by adjusting the position of the device with respect to the objective of the microscope and repeating the cycle for different applied voltages. Here it is demonstrated to find only the tip deflections which are of major interest in this thesis. Each of these steps is explained in detail in the following subsections.

5.3.1 TEST SET UP

The test setup consists of an optical microscope and an imaging camera for visualizing the moving device, ocular micrometer to measure the static deflection, DC step up transformer and DC power supply to give power for the actuation. All the details of the test setup are clearly labeled in the Figure 5.1. The MEMS device is mounted in the field of view of the optical microscope. The device is placed sideways as shown in this figure so that the gap between the electrodes and the out of plane deflections could be very clearly visualized, An ocular micrometer was attached to the microscope to quantitatively measure various moving positions and deflection of the tip of the actuator. The DC transformer is connected to the power supply and a multimeter is also connected in series for the measurement of actual voltage being applied on the actuator. The MEMS device is a cylindrical actuator, the details of which are presented in the following sub section.

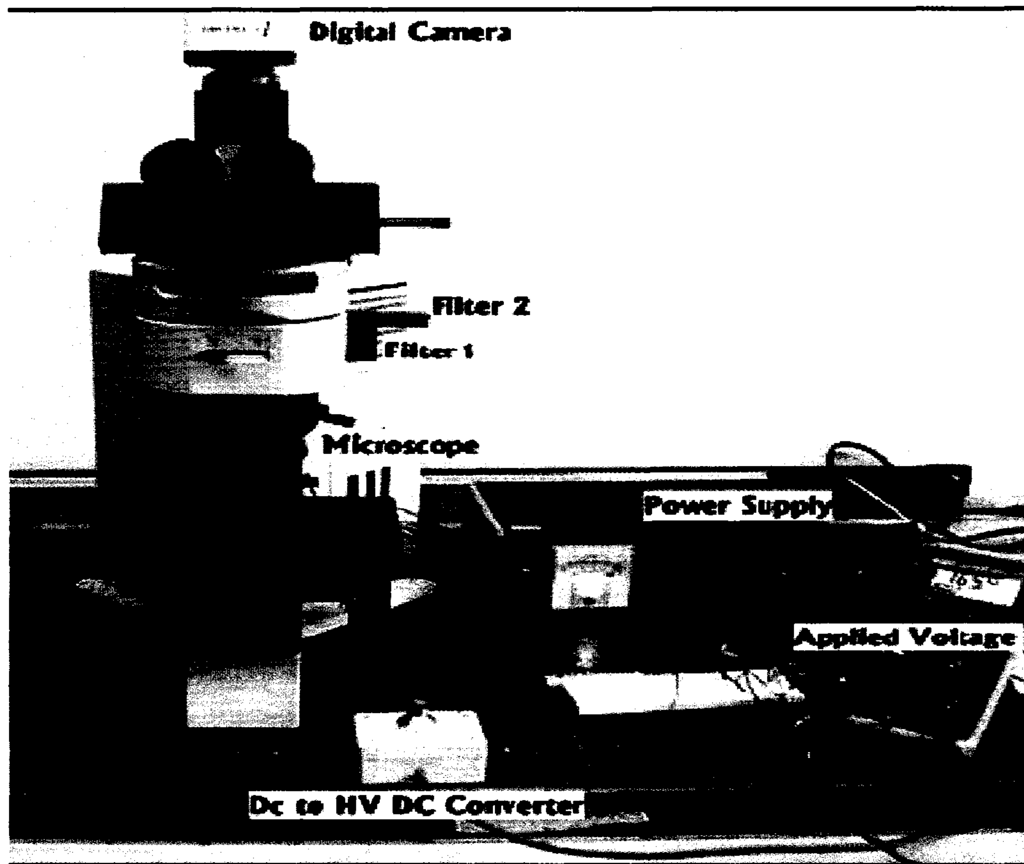

Figure 5.1: Experimental test set up for static deflection measurement

5.3.2 TEST DEVICE PREPARATION

Figure 5.2 shows the schematic of the prepared sample. The test device is very simple but it very well illustrates the actual device proposed in the design chapter. A glass substrate has been used as a substrate for mounting the device because it offers least electrostatic charges and fields that can interfere with the induced electrostatic fields while the voltages are applied. A copper tape has been attached on the top of glass substrate which forms the bottom electrode for the electrostatic actuation. A double sided sticky tape of thickness 76 microns has been applied on the top of this copper electrode to

form the insulation layer between the two electrodes. A multimode fiber coated with metal (Aluminium) is attached on the top surface of the sticky insulation layer. The fiber of the required length is cut using a special cleaver that does not bend the fiber while cutting. The fiber is carefully and skillfully attached using tweezers on the top of insulation layer in such a way that only required length of the fiber overhangs over the insulation layer and also forms the top electrode. Both the electrodes have been soldered and connectorised with electrical wires for electrical circuit. The electrical continuity is checked with the help of a multimeter. Finally the device consisting of the mechanical structure and the electrodes with electrical pins for actuation is prepared. Ideally the gap between the two electrodes is equal to the thickness of the insulation layer but since the fiber was a little curved upwards it was varying and had to be measured using the microscope and hence the gap was hard to control in the experiments. However average gap has been considered in the calculations for theoretical comparisons. The device under test along with the test setup is shown in Figure 5.3. Two devices were fabricated and tested. The real dimensions of the devices used for modeling and comparison are given in Table 5.1.

Table 5.1: Property values and dimensions of waveguides used in experiments.

	Device S	Device L
Length	15 mm	20 mm
Electrode gap	150 microns	180 microns
Youngs modulus	70 GPa	70 GPa
Coating Diameter	170 microns	170 microns
Fiber diameter	113 microns	113 microns
density	2200 kg/m^3	2200 kg/m^3

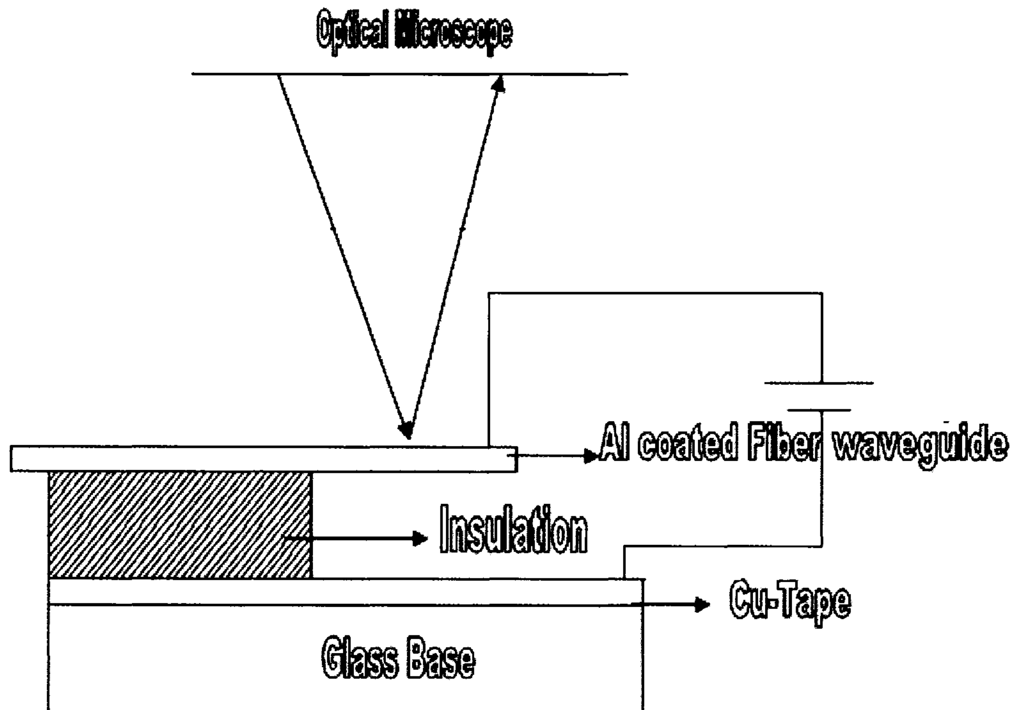

Figure 5.2 : Schematic of the experimental static deflection test setup

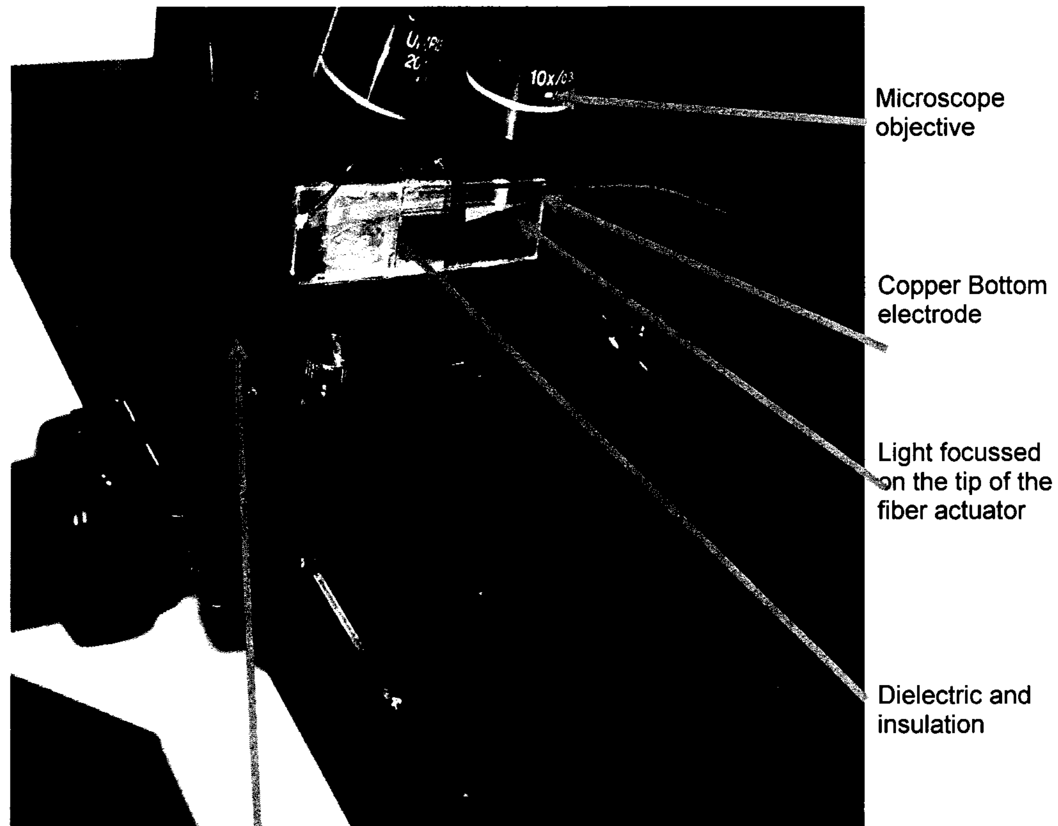

Figure 5.3: Close up of the MEMS VOA device under test.

5.3.3 MEASUREMENT OF TIP DEFLECTION

The graduations on the ocular micrometer are used to reference the tip of the actuator under no applied voltage. As a DC voltage is applied, the actuator moves to a new position. The tip focus is matched with a new graduation mark and the corresponding reading is noted for every voltage step applied as shown in the Table 5.2. The exact value of these graduations depends on the objective of the microscope used and are obtained by multiplying with a corresponding calibration.

Deflection or the actuation is obtained by the simple formula,

$$\text{Tip Deflection} = [\text{Value_voltage} - \text{Value_reference}]*\text{CF} \quad (5.1)$$

Where,

Value_voltage is the position reading of the tip at applied voltage, Value_reference is the value under no voltage, and CF is the calibration factor. Since a 10X zoom microscopic objective was used, the calibration factor is 2 in this case.

Table 5.2: Experimental measurements on the ocular of the microscope for a 15 mm fiber actuator Devices.

VOLTAGE (V)	Tip Deflection (μm)
0	0
80	2
134	4
153	6
175	8
190	10
210	12
226	14
237	16
251	18
264	20
275	22
284	24
292	26
303	28
309	30
317	32
324	34
329	36
339	40
350	44
351	44.5
358	48
361	52
371	58
375	60
378	64
381	70
383	74
386	160

5.4 RESULTS, OBSERVATIONS AND DISCUSSIONS

Actuators of two different lengths 15 and 20 mm have been used for the experimental testing. These particular lengths have been selected for the experiments so as to meet the voltages limitations of the DC power supply. The dimensions and material properties of the test devices used were given in Table 5.1. In order to compare theoretical and experimental results, the model from Chapter 2 has been used considering the parameters from the Table 5.1. The boundary condition of the fiber waveguide fixed on the tape is close to the fixed end condition of a cantilever and hence the same has been used in the theoretical validation. As already mentioned the electrode gap was hard to measure and was varying along the length and hence an average gap was used for the calculation. The results obtained from the experiment and theory, and their comparison are presented in the Figure 5.4 and Figure 5.5 and it can be clearly seen that both follow the same trend of increasing deflection with applied voltages. The deflections obtained from the experiments are very close to the theoretical results.

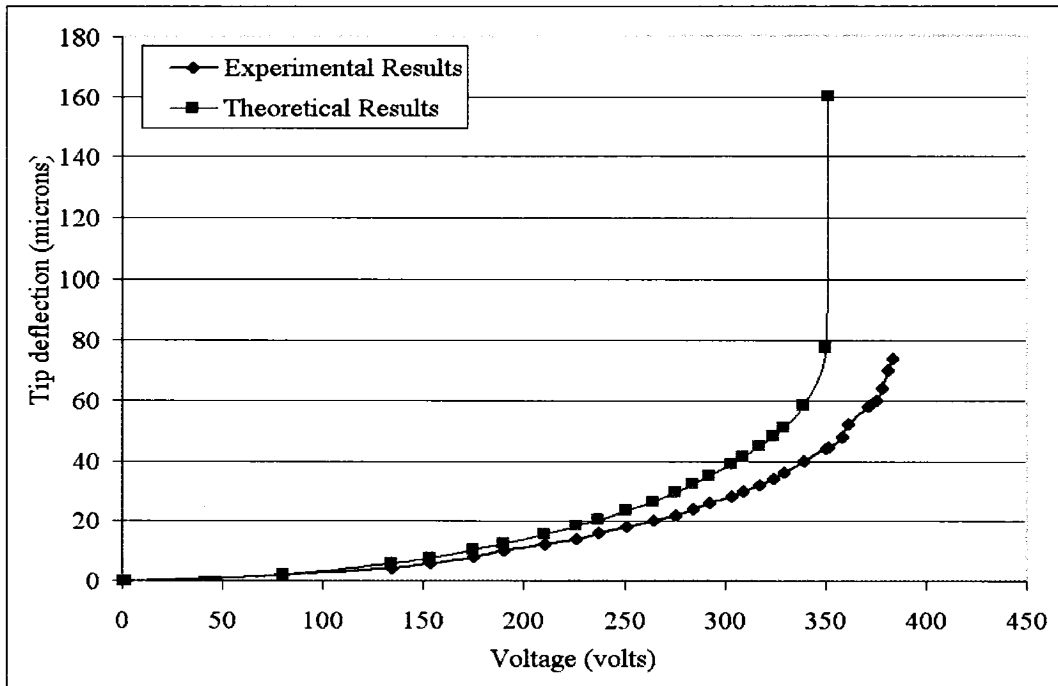

Figure 5.4: Variation of tip deflection against applied voltage for the Design S

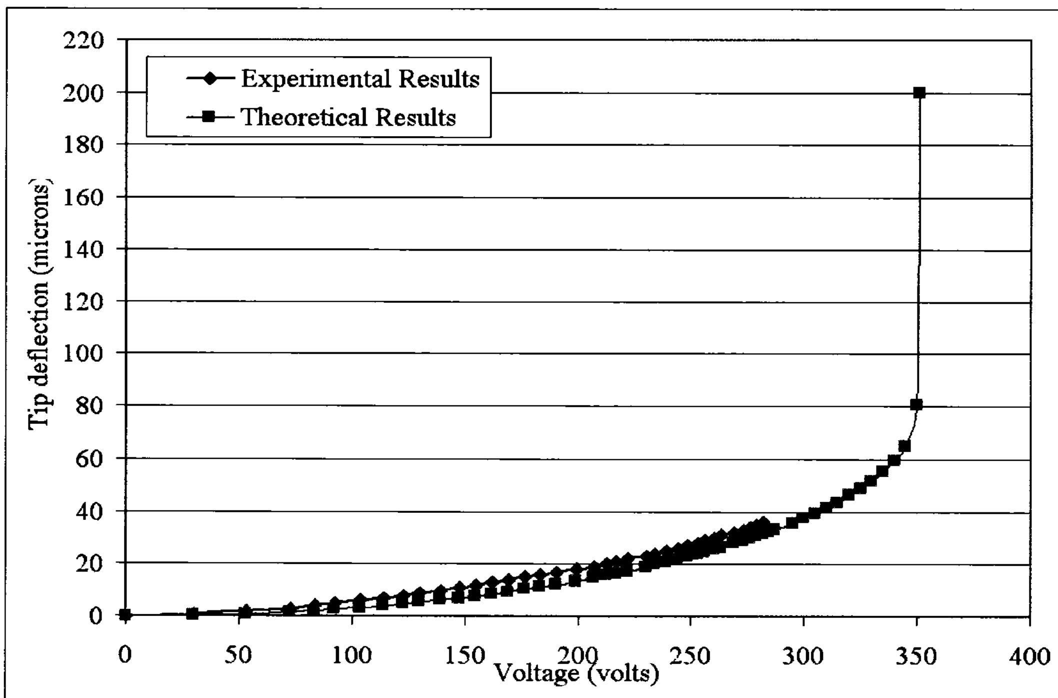

Figure 5.5: Variation of tip deflection against applied voltage for the Design L

When the applied voltage was increased beyond a certain level and close to the pull-in voltage the fiber started vibrating about the mean position. This is due to the pull-in instability of the system where the electrostatic force and the mechanical force dominate alternatively and each takes a turn in being the highest value. This leads to the vibration of the cantilever. As voltage was further increased the vibration amplitude increased further and also few electric sparks were observed while the cantilever was moving closer to the bottom electrode. These sparks are due to the discharge of electric field from positive charged electrode to the negative charged electrode. Figure 5.6 shows the spark due to electric discharge. It can be seen from the figure that the sparks occurred at locations away from the tip of the actuator. This confirms the presence of higher modeshapes in the vibrating actuator where the highest amplitude can be at any point along he length of the cantilever beam. Also burns could be observed around the end region of the cantilever which is from the intense heat generated as a result of the touch down phenomenon. This could cause higher currents to pass all over the circuit and damage the devices and hence a safety circuit consisting of a very high value resistor and LED was used to protect the equipment. The multimeter was also showing a voltage of 0 and the Pull in voltage alternatively which corresponds to the unstable equilibrium of the system from mechanical and electrostatic forces. As the voltage was increased a little further, the electric force became the dominant force and finally the fiber was observed to touch down. Also no hysterisis was observed when the voltages were decreased back in the same order as almost the same values of deflection were obtained. Now that the testing procedure gave insight into the static behaviour of the system, next phase is to understand the dynamic behaviour of the system which is described in the next section.

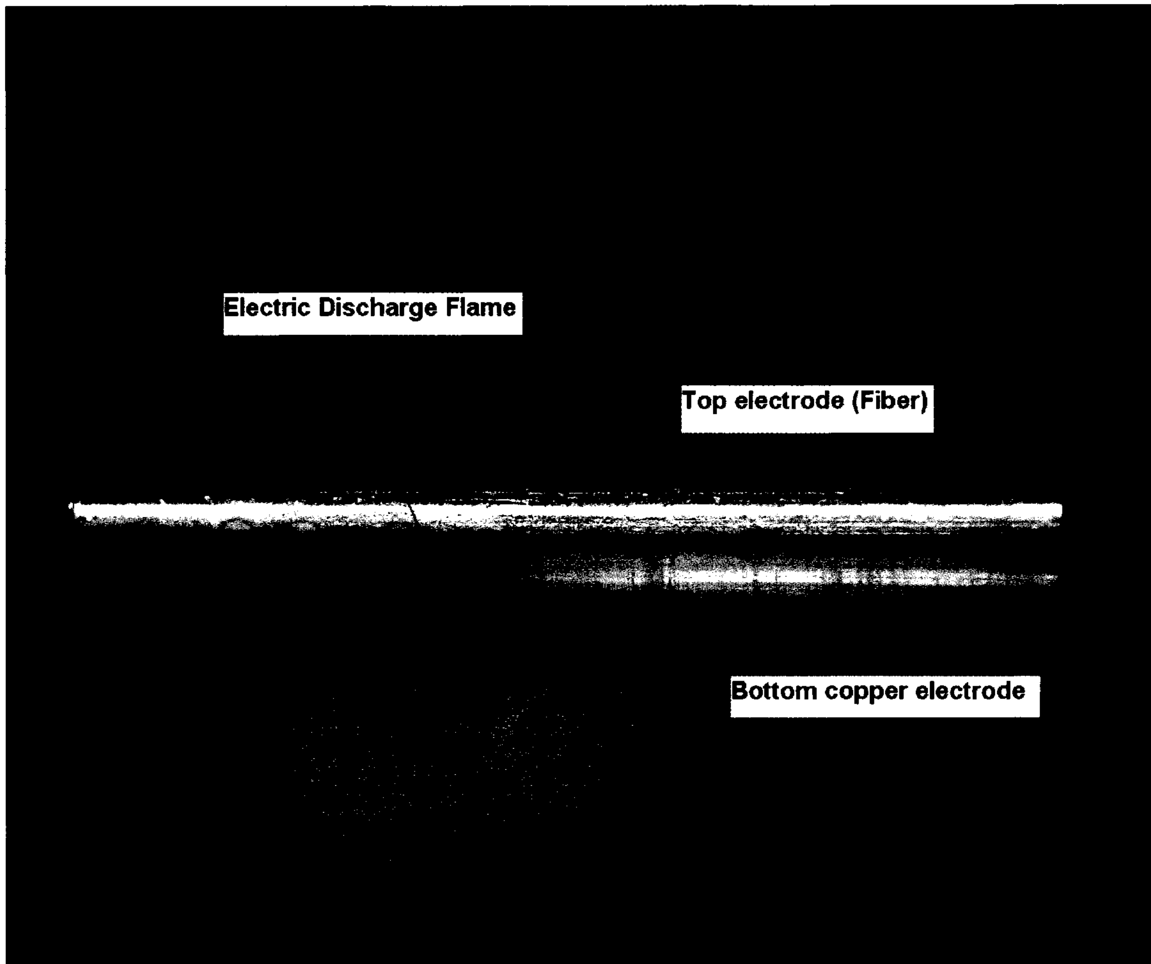

Figure 5.6: Flames appearing due to the Electric discharge when the top electrode approaches bottom electrode.

5.5 DYNAMIC TESTING

To completely validate the modeling and simulations in their initial phase of design dynamic testing is very important. Dynamic testing involves two parts: excitation of the sample using a source of excitation and measurement of the frequency of excitation using optics. Various practical excitation sources are generally used, such as, acoustic speaker, piezoelectric excitation and predefined AC signal. The latter has been used as a source of excitation in this work because of its simplicity and ease of control. The measurement of

the excitation is carried using the principle of Laser Doppler Velocimetry which works on the principle of Doppler shift. This principle uses the frequency shift of the light that occurs when there is a relative motion between the source and observer, which is the reflecting surface on the moving device here.

5.5.1 TEST SETUP

Figure 5.7 and Figure 5.8 show the test setup used for the measurement of the vibration of cylindrical micro actuators. The experimental test set up consists of a commercial Bruel and Kjaer Laser Doppler Velocimetry (LDV) equipment, combination of converging and diverging lens for alignment of the laser beam and the MEMS device held on an adjustable platform, all aligned in line relatively to each other on an optical table used for isolating external noise and vibrations [79]. The LDV module has a built in He Ne laser source that emits a coherent laser beam of red color wavelength and a photo detector for capturing the reflected signal from the vibrating MEMS device .The laser beam from the LDV passes through the converging diverging lens which adjust the intensity of the light sufficient enough to get reflected from the moving device. The MEMS device is held on a movable platform which could be adjusted in line to the laser beam path. The light reflected from the device passes back through the LDV and the reflected wavelength is compared with a reference signal to evaluate the phase shift. This could be measured from the output signal obtained by connecting LDV to the oscilloscope. The output signal is also monitored by a spectrum analyzer as can be seen from the Figure 5.7.

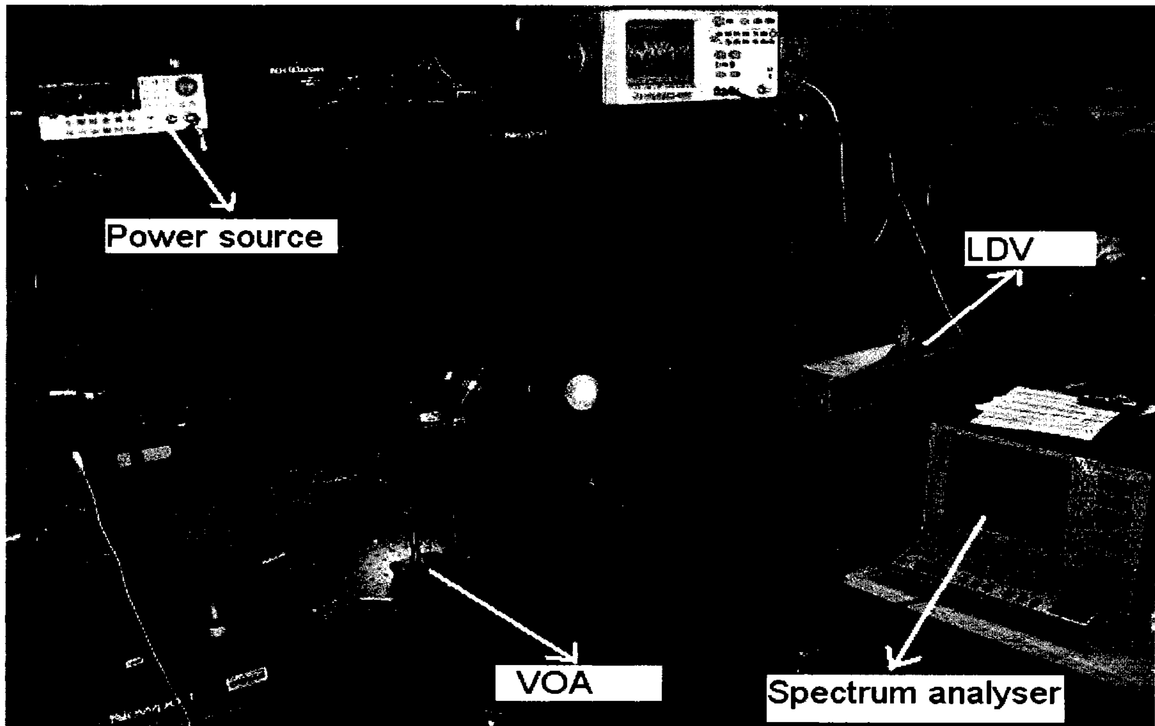

Figure 5.7 : Testing setup using Laser Doppler Velocimetry.

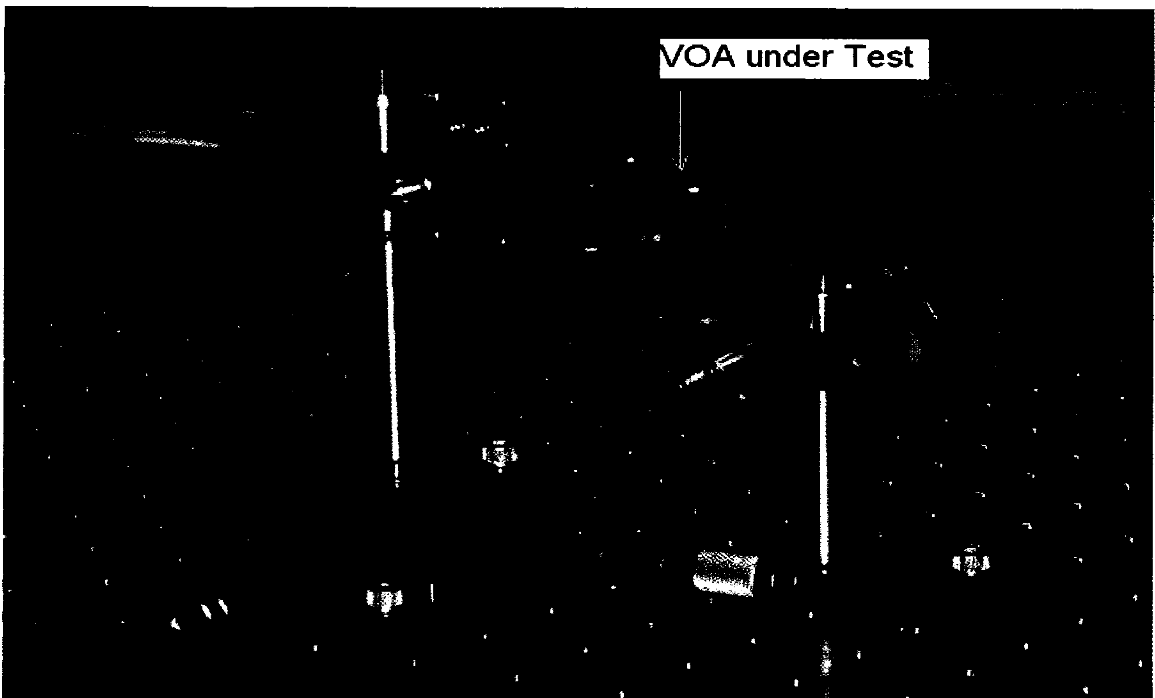

Figure 5.8: Close up view of the device mounted on an xyz positioner for aligning with the Laser

5.5.2 TESTING PROCEDURE

The frequency response of the VOA device Design S has been obtained using the spectrum analyzer for a particular test length of the beam by sweeping a wide range of frequencies in the function generator. Measuring the response signal was hard because of the cylindrical curvature of the beam and hence major part of the laser beam was scattered and reflected everywhere and relatively small portion of the light is reflected back into the LDV. Hence a small reflective tape was added as shown in Figure 5.9 at the tip of the cantilever in order to circumvent the problem. The effect of the addition of this mass would result in decrease of the natural frequency and hence this effect was also considered in the theoretical modeling discussed in Chapter 3. The tape was considered as an additional lumped mass at the tip of the beam in theoretical modeling and its influence was incorporated by an additional kinetic energy due to this tape given by the equation.

$$T_{tape} = \frac{1}{2} m_{tape} y^{1}(x = 0.9)^{2} \tag{5.1}$$

Where x = 0.9 corresponds to the exact non dimensionalised position of the tape with respect to the length of the beam.

The corresponding additional term in the mass matrix of the eigenvalue problem in Chapter 3 is given by

$$M_{tape}^{(i,n)} = m_{tape} \phi_i (x = 0.9) \phi_j (x = 0.9) \tag{5.2}$$

This additional term will be added to the existing mass matrix in Equation (3.14) and hence the new mass matrix in the eigenvalue problem would be given as

$$M = M^{(i,n)} + M_{tape}^{(i,n)} \tag{5.3}$$

The property of the tape used for calculation is given in Table 5.3.

Table 5.3: Dimensions and mechanical properties of the reflective tape

Area of the reflective tape used	4.5 mm^2
Density	0.80 gram/cc
Thickness	0.1 mm
Position of the tape from the fixed end	13.5 mm

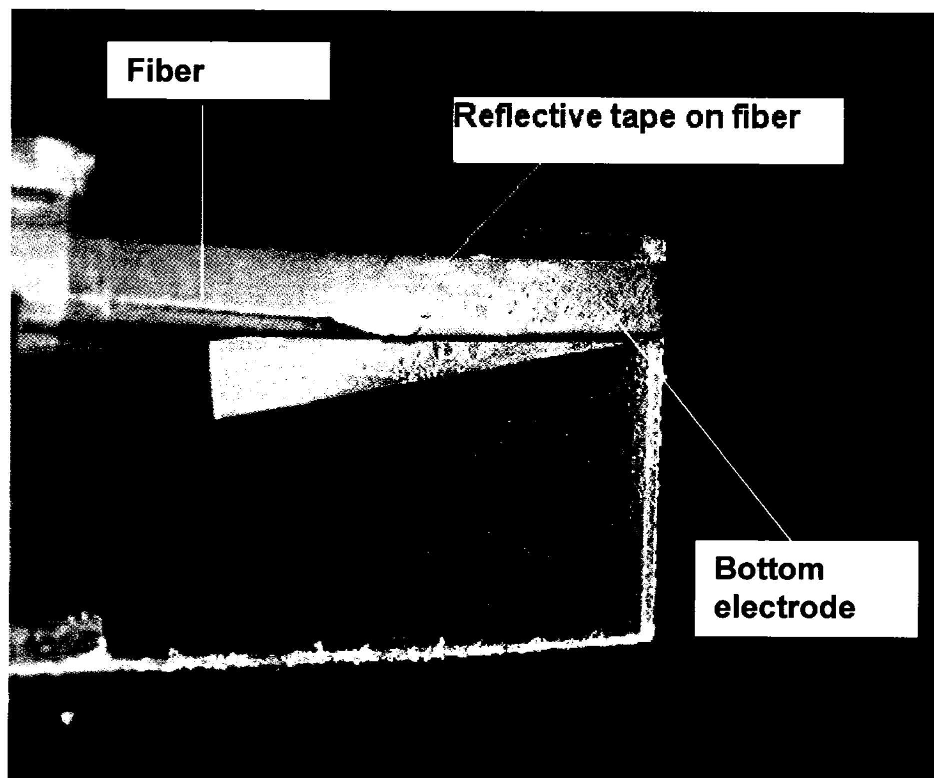

Figure 5.9: Reflective tape used to increase the intensity of the reflected laser beam signal

5.6 RESULTS AND DISCUSSIONS

The frequency response obtained from the excitation of the fiber to an AC excitation is shown in the Figure 5.10. A very clear and distinct peak could be observed at 292 Hz. This corresponds to the first natural frequency of the Device S. The theoretical model adapted to fit the real test scenario by the addition of a lumped mass has predicted a resonance at 236 Hz. Both the results are very close and this confirms the theoretical model.

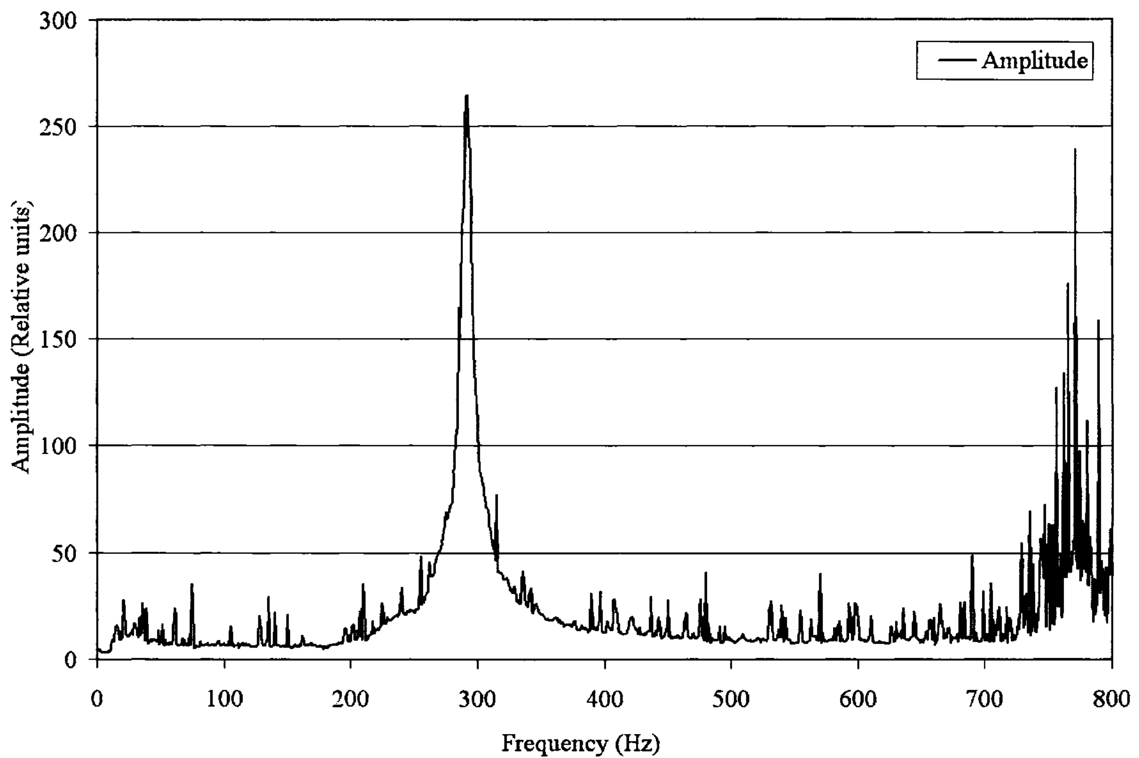

Figure 5.10: Frequency response of Device S with electrostatic excitation

Table 5.4: Comparison of natural frequencies for Device S

	Experimental (Hz)	Theoretical (Hz)
First natural frequency	292	236

5.7 SUMMARY

The literature on MEMS testing methods has been discussed. Method of static testing using direct visual inspection by optical microscope has been presented. The test setup and the preparation of the test device have been described. The static deflections have been evaluated for various dimensions of test devices. Interesting observations of electrostatic actuation including spark resulting from electric discharge and the touch down have been shown .Theoretical model has been used to find the static deflection of the tested device. Both experimental and theoretical results were found to conform well each other. Dynamic testing using LDV has been discussed. The problems and limitations associated with using this method for the cylindrical actuators and ways of circumventing them have been discussed. Finally, test results have been compared with theoretical results. Both the methods of testing could be used to measure all along the length of the beam and can give a complete 3d characterization. Testing gave an insight into the realities of the proposed scheme and gave feedback on the quality of theories used in modeling and assumptions made in the process. This could be used to further study the behaviour and control the actuation scheme in a more refined way.

CHAPTER 6

CONCLUSIONS, CONTRIBUTIONS AND RECOMMENDATIONS FOR FUTURE WORK

6.1 CONCLUSIONS

A novel electrostatically actuated waveguide based VOA with a dynamic range of attenuation has been proposed. Both electromechanical and optical models have been established. Optical attenuation over a continuous range of 30 dB has been demonstrated using reasonable applied voltages below 50 Volts. Also, the attenuation characteristics of the system with varying critical design parameters of voltage, length and electrode gap have been demonstrated. The effect of pull-in voltage on the possible range of attenuation has been studied. The parametric study gave insight into the design procedure for the proposed attenuation scheme. The electrode gap primarily determined the range of possible actuation and had to be varied according to the range of attenuation required. Further the length of the fiber can be varied according to the constraints of available voltage range. Due to the nonlinear nature of the attenuation with applied voltage, the VOA has to be calibrated initially. This work demonstrated theoretically the possibility of an optical attenuator by electrostatically actuated cylindrical waveguide.

An introduction to electrostatic actuation and its applications was given. Various issues of modeling electrostatic actuators like nonlinearity, pull in and electromechanical coupling have been explained in detail and the ways of addressing them in the modeling procedures have been explained. The static modeling using nonlinear electromechanical model that takes into consideration of all these effects and

also the geometry of the electrodes has been proposed. The model was proved to be accurate by the comparison of the tip deflection of a cantilever which was found to be in good agreement with literature. The model was very well demonstrated on nano scale with the application on a nano actuator.

Dynamic modeling to find the natural frequencies and the mode shapes of the cantilever was also presented. Rayleigh Ritz energy method has been used for the coupled electromechanical modeling. Gram Schmidt orthogonolization method of generating polynomials for achieving higher accuracy of the fundamental natural frequency and obtaining the higher mode shapes has been discussed. The softening of the structure due to the negative stiffness of the electrostatic field was observed. The elastic foundation method has been used for small amplitude vibrations. The pull-in voltages of the electrostatically actuated waveguides have been predicted by the model. The results from the model can be used in the design process of the VOA to avoid resonance and snap down of the structures which are critical properties that limit the functionality of the VOA.

The static testing of the test device under optical microscope has been very successful in determining the tip deflection of the cantilever which is emphasized by the close match between experimental and theoretical results. Pull in phenomenon of electrostatic actuation has been very well visualized. It was inferred that the pull in point is close to half of the electrode gap and not one third of the gap. This distinguishes the cylindrical actuation from the parallel plate actuation. Dynamic testing using Laser Doppler Velocimetry has been good enough in finding the fundamental frequencies of the

actuator. Problems like laser scatter were avoided using an enhanced reflective tape. Though approximate, it was effective enough in evaluating the theoretical dynamic model.

6.2 CONTRIBUTIONS

The contributions of this thesis work can be highlighted in brief as,

1. Successfully proposed and established the proof of concept of a simple and novel MEMS based variable optical attenuator capable of continuous attenuation with a dynamic range of 0 to 30dB.

2. Accurately developed models to define the static, dynamic and optical behaviour of MEMS devices.

3. Developed an efficient computational design methodology using Rayleigh Ritz energy method and deflection approximations.

4. Demonstrated the electromechanical model for various applications containing cylindrical actuators.

5. Experimental test setups and methodologies have been established for the static and dynamic testing of cylindrical actuators

6. The phenomenon of pull in has been very well visualized which includes electric discharges and sparks generated at the end of the moving device which is a direct feedback for further modeling enhancements.

7. A comprehensive review of various driving principles and mechanisms of VOAs and their role in telecommunications has been concisely presented.

8. Various existing methods of modeling electrostatic actuation have been outlined

6.3 RECOMMENDATIONS FOR FUTURE WORK

The present work has proposed a new design and has discussed the synthesis of the microsystem to establish the proof of the concept. But there is more work to be done in making the design robust and in realizing the proposed device. This work can be subject to further study and analysis and the following ideas give direction to future work.

1. Experimental Optical testing of the device by coupling the light from the moving input waveguide to the output waveguide coupled to a detecting photo detector for evaluation of intensity to confirm the optical models and attenuation range.
2. Low response time of less than 1 microsecond of these VOAs can permit real time closed loop control systems. Implementation of a closed circuit for feedback would lead to a more stable system.
3. Experimental dynamic modeling by varying the DC voltage along with the AC voltage would give the natural frequencies of VOAs for various attenuation levels.
4. Also the device could be fabricated in a V groove to emulate the proposed device and facilitate real testing and boundary characterization.
5. Optimization of the design

REFERENCES

[1] W.J. Pulliam, P.M. Russler, R.S. Fielder, High-temperature high-bandwidth fiber optic MEMS pressure-sensor technology for turbine-engine component testing, Proceedings of SPIE 4578 (2001) 229–238.

[2] A.H. Epstein, Millimeter-Scale, Micro-Electro-Mechanical Systems Gas Turbine Engines, Journal of Engineering for Gas Turbines and Power 126 (2004) 205.

[3] S.E. Lyshevski, Nano-and Micro-electromechanical Systems: Fundamentals of Nano- and Microengineering, CRC Press, 2005.

[4] M.E. Motamedi (Ed.), Micro-Opto-Electro-Mechanical Systems, SPIE, 2005.

[5] F. Strong, J. Skinner, A. Talin, P. Dentinger, N. Tien, Electrical Breakdown Response for Multiple-Gap MEMS Structures, Reliability Physics Symposium Proceedings, 2006.44th Annual., IEEE International (2006) 421-426.

[6] D. Elata, O. Bochobza-Degani, Y. Nemirovsky, A micromirror device with post-fabrication re-adjustable pull-in parameters, TRANSDUCERS, Solid-State Sensors, Actuators and Microsystems, 12th International Conference on, 2003 2 (2003) .

[7] D.R. Goff, Fiber Optic Reference Guide: A Practical Guide to Communications Technology, Focal Press, 2002.

[8] John S. McKillop, Applications of MEMS in Telecommunications, Published Report.

[9] T. Kowalczyk, I. Finkelshtein, M. Kouchnir, Y. Lee, A.D. Nguyen, D. Vroom, W. Bischel, Variable optical attenuator with large dynamic range and low drive power, Optical Fiber Communication Conference and Exhibit, 2001.OFC 2001 3 (2001) .

[10] C. Wang, H. Li, J. Fang, D. Zhang, S. Chang, Design and fabrication of a novel micromechanical variable optical attenuator, Proceedings of SPIE 4601 (2003) 428.

[11] K. Ishikawa, Q. Yu, An Integrated AWG multi/demultiplexer with MEMS-VOA shutters, Thermal and Thermomechanical Phenomena in Electronic Systems, 2004.ITHERM'04.The Ninth Intersociety Conference on 2 (2004) .

[12] S. Kim, S. Nam, Novel MEMS variable optical attenuator with expanded core waveguides, Optical MEMs, 2002.Conference Digest.2002 IEEE/LEOS International Conference on (2002) 65-66.

[13] X. Dai, X. Zhao, B. Cai, Development and characterization of electromagnetic micro shutter in MEMS variable optical attenuator, Optical MEMs, 2002.Conference Digest.2002 IEEE/LEOS International Conference on (2002) 63-64.

[14] J. Chiou, W. Lin, Variable optical attenuator using a thermal actuator array with dual shutters, Opt. Commun. 237 (2004) 341-350.

[15] C. Lee, Y.J. Lai, Y.S. Lin, C.Y. Wu, C. Chen, M.H. Tasi, S.Y. Hung, Y.M. Huang, R.S. Huang, M.S. Lin, Development of Surface Micromachined Mechanism for Movement Translation and Displacement Amplification, Japanese Journal of Applied Physics 43 (2004) 3887-3891.

[16] Y.J. Lai, C.Y. Wu, C. Lee, Y.S. Lin, W.C. Chen, C. Chen, M.H. Tsai, R.S. Huang, M.S. Lin, A.P.M. Inc, Out-of-plane MEMS shutter with continuous motion capability for VOA application, Lasers and Electro-Optics, 2003.CLEO/Pacific Rim 2003.The 5th Pacific Rim Conference on 1 (2003) .

[17] C. Lee, Y.J. Lai, C.Y. Wu, Y.S. Lin, M.H. Tasi, R.S. Huang, M.S. Lin, Scratch Drive Actuator Driven Self-assembled Variable Optical Attenuator, Japanese Journal of Applied Physics 43 (2004) 3906-3909.

[18] R. Syms, H. Zou, J. Stagg, H. Veladi, Sliding-blade MEMS iris and variable optical attenuator, J Micromech Microengineering 14 (2004) 1700-1710.

[19] C. Marxer, P. Griss, N. de Rooij, A variable optical attenuator based on silicon micromechanics, Photonics Technology Letters, IEEE 11 (1999) 233-235.

[20] C.H. Ji, Y. Yee, J. Choi, J.U. Bu, Electromagnetic variable optical attenuator, Optical MEMs, 2002.Conference Digest.2002 IEEE/LEOS International Conference on (2002) 49-50.

[21] T.H. Kim, H.N. Kwon, J.Y. Hong, J.H. Lee, 2× 2 bi-reflection optical add-drop module with variable attenuation using four 45° micromirrors, Proceedings of SPIE 5719 (2005) 23.

[22] C. Chen, C. Lee, J.A. Yeh, Retro-reflection type MOEMS VOA, IEEE Photonics Technology Letters 16 (2004) 2290-2292.

[23] J. Ford, J. Walker, D. Greywall, K. Goossen, Micromechanical fiber-optic attenuator with 3 μs response, Journal of Lightwave Technology, 16 (1998) 1663-1670.

[24] R. Syms, H. Zou, J. Stagg, D. Moore, Multistate latching MEMS variable optical attenuator, Photonics Technology Letters, IEEE 16 (2004) 191-193.

[25] Q. Li, A. Au, C.H. Lin, E. Lyons, H. Lee, An efficient all-fiber variable optical attenuator via acoustoopticmode coupling, Photonics Technology Letters, IEEE 14 (2002) 1563-1565.

[26] J.J. Choi, D.Y. Kim, G.T. Park, H.E. Kim, Electro-Optic Properties of PLZT Thick-Film on Glass Substrate with Embedded Electrodes Structure, Journal of the Korean Physical Society 42 (2003) S1310-S1312.

[27] Y. Zou, J.J. He, S. He, Analysis and optimization of an InGaAsP/InP waveguide variable optical attenuator, Opt. Commun. 262 (2006) 188-192.

[28] Y. Noh, M.S. Yang, Y. Won, W.Y. Hwang, PLC-type variable optical attenuator operated at low electricalpower, Electron. Lett. 36 (2000) 2032-2033.

[29] W. Lee, W. Shin, H. Seo, K. Oh, Achievement of uniform attenuation from 1.25 to 1.6 μm using anew three-layered Co 2 doped optical fiber, Photonics Technology Letters, IEEE 13 (2001) 1322-1324.

[30] A. Zohrabyan, D. Dumont, A. Tork, R. Birabassov, T. Galstian, In-fiber variable optical attenuation with ultra-low electrical power consumption, Proceedings of SPIE 5724 (2005) 124.

[31] Y. Kikuya, M. Hirano, K. Koyabu, F. Ohira, Alignment of optical axes by using electrostatic force, Opt. Lett. 18 (1993) 864-866.

[32] Y.J. Yang, W.C. Kuo, K.C. Fan, W.L. Lin, A 1× 2 optical fiber switch using a dual-thickness SOI process, J Micromech Microengineering 17 (2007) 1034-1041.

[33] H. Willis, Advanced Process Control, McGraw-Hill, 1981.

[34] J.A. Pelesko, D.H. Bernstein, Modeling Mems and Nems, CRC Press, 2003.

[35] P. Bruschi, A. Nannini, F. Pieri, G. Raffaa, B. Vigna, S. Zerbini, Electrostatic analysis of a comb-finger actuator with Schwarz–Christoffel conformal mapping, Sensors and Actuators A 113 (2004) 106-117.

[36] M. Younis, E. Abdel-Rahman, A. Nayfeh, A reduced-order model for electrically actuated microbeam-based MEMS, Journal of Microelectromechanical Systems, 12 (2003) 672-680.

[37] G. Li, N. Aluru, Efficient mixed-domain analysis of electrostatic MEMS, Computer-Aided Design of Integrated Circuits and Systems, IEEE Transactions on 22 (2003) 1228-1242.

[38] P.C.P. Chao, C. Chiu, C. Tsai, A novel method to predict the pull-in voltage in a closed form for micro-plates actuated by a distributed electrostatic force, J.Micromech.Microeng 16 (2006) 986-998.

[39] A. Collenz, F.D. Bona, A. Gugliotta, A. Soma, Large deflections of microbeams under electrostatic loads, J Micromech Microengineering 14 (2004) 365-373.

[40] G. Ananthasuresh, Optimal Synthesis Methods for MEMS, Kluwer Academic Publishers, 2003.

[41] J.H. Kane, Boundary element analysis in engineering continuum mechanics, Englewood Cliffs, NJ: Prentice Hall, (1994) .

[42] S.D. Senturia, Microsystem design, Kluwer academic publishers, 2004.

[43] Y. Nemirovsky, O. Bochobza-Degani, A methodology and model for the pull-in parameters of electrostaticactuators, Journal of Microelectromechanical Systems, 10 (2001) 601-615.

[44] G. Lorenz, R. Neul, S. Dickmann, Modeling of Electrostatic MEMS Components, Proc.2.Int.Conf.on Modeling and Simulation of Microsystems, MSM99, San Juan (1999) 128-131.

[45] W.H. Hayt, Engineering electromagnetics, McGraw-Hill New York, 2001.

[46] I.H. Shames, C.L. Dym, Energy and Finite Element Methods in Structural Mechanics, Hemisphere, 1985.

[47] A.K. Bhaskar, M. Packirisamy, R.B. Bhat, Modeling switching response of torsional micromirrors for optical microsystems, Mechanism and Machine Theory 39 (2004) 1399-1410.

[48] G.T.A. Kovacs, Micromachined transducers sourcebook, McGraw-Hill Boston, 1998.

[49] M. Dequesnes, S. Rotkin, N. Aluru, Calculation of pull-in voltages for carbon-nanotube-based nanoelectromechanical switches, Nanotechnology 13 (2002) 120-131.

[50] S. De, N. Aluru, Full-Lagrangian schemes for dynamic analysis of electrostatic MEMS, Journal of Microelectromechanical Systems, 13 (2004) 737-758.

[51] Y. He, J. Marchetti, C. Gallegos, F. Maseeh, Accurate fully-coupled natural frequency shift of MEMS actuatorsdue to voltage bias and other external forces, Twelfth IEEE International Conference on Micro Electro Mechanical Systems, MEMS'99. (1999) 321-325.

[52] L. Rocha, E. Cretu, R. Wolffenbuttel, Behavioural analysis of the pull-in dynamic transition, J Micromech Microeng 14 (2004) 37-42.

[53] O. Français, G.E. ELMI, B.B. Pascal, Analysis of an Electrostatic Microactuator with the help of Matlab/simulink: transient and frequency characteristics, MSM2000, San Diego, CA, USA (2000) 281-284.

[54] J. Seeger, S. Crary, Stabilization of electrostatically actuated mechanical devices, International Conference on Solid State Sensors and Actuators, TRANSDUCERS'97 Chicago., 2 (1997) .

[55] K.S. Chen, K.S. Ou, Development and verification of 2D dynamic electromechanical coupling solver for micro-electrostatic-actuator applications, Sensors and Actuators A: Physical 136 (2007) 403-411.

[56] G. Rinaldi, M. Packirisamy, I. Stiharu, Geometrical Performance Conditioning of Microstructures, ISSS Conference on Smart Materials, Structures and Systems, July 28 - 30, 2005, Bangalore, India..

[57] R.B. Bhat, Nature Of Stationarity Of the Natural Frequencies at the Natural Modes in the Rayleigh-Ritz Method, J. Sound Vibratio. 203 (1997) 251-263.

[58] G. Mundkur, R.B. Bhat, S. Neriya, Vibration of plates with cut-outs using boundary characteristic orthogonal polynomial functions in the Rayleigh-Ritz method, J. Sound Vibrat. 176 (1994) 136-44.

[59] R. Bhat, Natural frequencies of rectangular plates using characteristic orthogonal polynomials in Rayleigh-Ritz method, J. Sound Vibrat. 102 (1985) 493-499.

[60] P. Poncharal, Electrostatic Deflections and Electromechanical Resonances of Carbon Nanotubes, Science 283 (1999) 1513-1516.

[61] R. Neul, Modeling and Simulation for MEMS Design, Industrial Requirements, Robert Bosch GmbH, Stuttgart, Germany.

[62] S.R. Pendyala, M. Packirisamy, I. Stiharu, N. Sivakumar, V. Nerguizian, Modeling of electrostatically actuated cylindrical-waveguide-based optical microsystem, Proceedings of SPIE 5719 (2005) 30.

[63] R.R.A. Syms, J.R. Cozens, Optical guided waves and devices, McGraw-Hill New York, 1992.

[64] I. De Wolf, Instrumentation and methodology for MEMS testing, reliability assessment and failure analysis, 24th International Conference on Microelectronics, 1 (2004) .

[65] F. M. Serry, T. A. Stout, M. J. Zecchino,C. Ragan, P. A. Browne, 3D MEMS Metrology with Optical Profilers, (2006) .

[66] J. Kung, H.S. Lee, R. Howe, A digital readout technique for capacitive sensor applications, IEEE Journal of Solid-State Circuits, 23 (1988) 972-977.

[67] S. Ranganathan, M. Inerfield, S. Roy, S.L. Garverick, Sub-femtofarad capacitive sensing for microfabricated transducers using correlated double sampling and delta modulation, IEEE Trans. Circuits Syst. II Analog Digital Signal Process. 47 (2000) 1170-76.

[68] A. Selvakumar, K. Najafi, A high-sensitivity z-axis capacitive silicon microaccelerometerwith a torsional suspension, Journal of Microelectromechanical Systems, 7 (1998) 192-200.

[69] J. Harkey, T. Kenny, 1/f noise considerations for the design and process optimization ofpiezoresistive cantilevers, Journal of Microelectromechanical Systems, 9 (2000) 226-235.

[70] R. Schnitzer, N. Ruemmler, V. Grosser, B. Michel, Vibration measurement of microstructures by means of laseroptical modal analysis, Proceedings of SPIE-The International Society for Optical Engineering 3825 (1999) 72–79.

[71] A. Bosseboeuf, J.P. Gilles, K. Danaie, R. Yahiaoui, M. Dupeux, J.P. Puissant, A. Chabrier, F. Fort, P. Coste, A versatile microscopic profilometer-vibrometer for static and dynamic characterization of micromechanical devices, Proc.SPIE 3825 (1999) 123-133.

[72] A. Bosseboeuf, S. Petitgrand, Characterization of the static and dynamic behaviour of M (O) EMS by optical techniques: status and trends, J.Micromech.Microeng 13 (2003) 23–33.

[73] G.T.A. Kovacs, Micromachined transducers sourcebook, WCB/McGraw-Hill, 1998.

[74] B. Borovic, A. Liu, D. Popa, H. Cai, F. Lewis, Open-loop versus closed-loop control of MEMS devices: choices and issues, J.Micromech.Microeng 15 (1917) 1924.

[75] K. Honer, N. Maluf, E. Martinez, G. Kovacs, Characterizing deflectable microstructures via a high-resolution laser-based measurement system, Sensors and Actuators A: Physical 52 (1996) 12-17.

[76] D. Jenkins, M. Cunningham, W. Clegg, M. Bakush, Measurement of the modal shapes of inhomogeneous cantilevers using optical beam deflection, Measurement Science and Technology 6 (1995) 160-166.

[77] G. Benedetto, R. Gavioso, R. Spagnolo, Measurement of microphone membrane displacement with an optical beam deflection technique, Rev. Sci. Instrum. 66 (1995) 5563.

[78] J. Hall, N. Apperson, B. Crozier, C. Xu, R. Richards, D. Bahr, C. Richards, A facility for characterizing the dynamic mechanical behavior of thin membranes for microelectromechanical systems, Rev. Sci. Instrum. 73 (2002) 2067.

[79] G. Rinaldi, M. Packirisamy, I. Stiharu, Dynamic testing of micromechanical structures under thermo-electro-mechanical influences, Measurement: Journal of the International Measurement Confederation 40 (2007) 563-574.